Seismogenic Fault Reactivation in Western Central Africa: Insights from Regional Stress Analyses

NKODIA Hardy Medry Dieu-Veill[1,1], Timothée Miyouna[2,2], Folarin Kolawole[3,3], Florent Boudzoumou[2,2], Rodeck Alan Patrick Loemba[2,2], Nicy Carmel Bazebizonza Tchiguina[4,4], and Damien Delvaux[5,5]

[1]Marien Ngouabi University
[2]Marien NGOUABI University, Faculty of Sciences and Technics, Department of Geology
[3]BP America
[4]Marien NGOUABI University, Faculty of Sciences and Technics
[5]Royal Museum for Central Africa

January 20, 2023

Abstract

The onshore continental margins of western Central Africa have been hosting potentially damaging earthquake events for decades; yet, the links between the seismicity, the contemporary stress field, and pre-existing faults are not well understood. Here, we analyze the regional stress fields along the coastal margin and interior cratonic areas using earthquake focal mechanisms, map and characterize the detailed structure of preexisting fault systems in outcrops, and assess the reactivation potential of the mapped structures. Our results show that the earthquakes originate under a transpressive stress regime with a horizontal maximum principal compressive stress ($\sigma 1$) that is oriented NNE-SSW. We show that regional stresses acting on offshore oceanic fracture zones are compatible with those acting along with the onshore areas of the continental margin. Field observations reveal the presence of large fault systems that deform both the Precambrian basement and Phanerozoic sedimentary sequences, with widespread hydrothermal alterations of calcite veining, quartz veining, and palygorskite mineralization along the fault zones. Along the margin, the preexisting NNE-, NNW-, and N-S -trending strike-slip faults and normal faults show a high slip tendency (60 – 100 %),), whereas in the cratonic interior, the NW- and N-S -trending thrust faults are the most likely to reactivate. We argue that favorable orientation of the preexisting faults and potentially, their hydrothermal alteration products, define the susceptibility of the faults to seismic reactivation. We propose that possible stress propagation into the near-shore and onshore tip zones of oceanic fracture zones may be driving stress loading on pre-stressed fault systems onshore.

Table S5. Coordinates of the field sites where the measurements were collected.

ID	Long	Lat	Area
Dbk	15,20794	-4,37181	Brazzaville and Kinshasa quarries
Dk	13,8508333	-4,29611111	Kolas Quarry
Dngov	14,91485	-5,31184	Ngovo Caves
Dwc1	12,58751	-4,185507	National Primary Road
Dso	14,15818	2,05411	Souanké Quarry

Table S3. Field measurements along the Dwc1 fault system, West Congo Belt, Republic of Congo and Democratic Republic of Congo.

Plane a recorded in Dip/Dip Direction convention

DataID	Type of structure	Plane	Line	Sense	Confidence
RDC-BC09-23	4	42/260		MJ	C
RDC-BC09-24	4	42/267		MJ	C
RDC-BC09-25	4	35/276		MJ	C
RDC-BC09-26	4	42/282		MJ	C
RDC-BC09-27	4	41/293		MJ	P
RDC-BC09-28	4	55/295		MJ	P
RDC-BC09-30	4	45/252		MJ	P
RDC-BC09-31	4	44/249		MJ	P
RC-CarriLesBandas-2	4	30/233		BJ	P
RC-CarriLesBandas-8	3	20/064	20/064	IX	C
RC-CarriLesBandas-9	3	10/064	10/064	IX	C
RC-CarriLesBandas-10	3	25/064	25/064	IX	C
RC-CarriLesBandas-11	3	24/064	24/064	IX	C
RC-CarriLesBandas-12	1	30/064	29/052	ID	C
RC-CarriLesBandas-13	1	30/065	29/053	ID	C
RC-CarriLesBandas-14	1	42/065	41/052	ID	C
RC-CarriLesBandas-15	1	35/062	34/050	ID	C
RC-CarriLesBandas-26-a	2	35/064	35/057	ID	P
RC-CarriLesBandas-26-b	2	30/233	30/241	IS	P
RC-CarriLesBandas-27-a	2	42/062	42/056	ID	P
RC-CarriLesBandas-27-b	2	30/233	30/240	IS	P
RC-CarriLesBandas-28-a	2	35/064	35/059	ID	P
RC-CarriLesBandas-28-b	2	40/238	40/243	IS	P
RC-CarriLesBandas-29-a	2	45/240	45/242	IS	P
RC-CarriLesBandas-29-b	2	35/062	35/060	ID	P
RC-CarriLesBandas-30-a	2	35/060	35/062	IS	P
RC-CarriLesBandas-30-b	2	45/242	45/240	ID	P
RC-CarriLesBandas-31-a	2	35/060	35/054	ID	P
RC-CarriLesBandas-31-b	2	45/233	45/239	IS	P
RC-Mvouti 1-entreeRN1-1	4	20/209		IJ	C
RC-Mvouti 1-entreeRN1-2	4	10/219		IJ	C
RC-Mvouti 1-entreeRN1-5	4	20/258		IJ	C
RC-Mvouti 1-entreeRN1-8	1	22/258	21/237	ID	C
RC-Mvouti 1-entreeRN1-9	1	20/209	19/230	IS	C
RC-Mvouti 1-entreeRN1-10	1	20/219	20/230	IS	C
RC-Mvouti 1-entreeRN1-23	1	62/232	57/267	IS	C
RC-Mvouti 1-entreeRN1-24	1	55/224	54/241	IS	C
RC-Moussouva RN-1	3	20/342	09/046	ND	C
RC-Moussouva RN-2	3	20/352	09/056	ND	C
RC-Moussouva RN-3	3	20/340	07/051	ND	C
RC-Moussouva RN-7	3	20/310	06/236	ID	P
RC-Moussouva RN-8	3	20/310	12/257	ID	P
RC-Moussouva RN-9	3	20/310	07/241	ID	P
RC-Moussouva RN-10	3	20/310	07/241	ID	P
RC-Moussouva RN-11	3	20/310	14/262	ID	P
RC-Moussouva RN-12	3	40/230	40/219	ID	P
RC-Moussouva RN-14	3	12/064	11/045	ID	P
RC-Moussouva RN-15	1	40/230	39/217	ID	P
RC-Moussouva RN-16	1	40/232	40/222	ID	P
RC-Moussouva RN-17	1	40/228	40/227	ID	P
RC-Moussouva RN-18	3	12/028	12/037	IS	P
RC-Moussouva RN-19	3	12/028	12/035	IS	P
RC-Moussouva RN-29	1	12/254	12/254	IX	C
RC-Moussouva RN-30	1	12/255	12/255	IX	C
RC-Moussouva RN-31	1	20/238	20/238	IX	C
RC-Moussouva RN-41	1	50/238	50/238	IX	C
RC-Moussouva RN-58	4	32/024		TJ	C
RC-Moussouva RN-59	4	24/042		TJ	C
RC-Moussouva RN-61	4	25/052		TJ	C
RC-Moukondo-RN1-1-a	2	32/290	32/290	IX	P
RC-Moukondo-RN1-1-b	2	22/110	22/110	IX	P
RC-Moukondo-RN1-2	1	32/254	32/254	IX	P
RC-Moukondo-RN1-3	1	15/128	14/111	ID	P
RC-Moukondo-RN1-4	1	20/119	20/111	ID	P
RC-Moukondo-RN1-5	1	11/132	10/112	ID	P
RC-Moukondo-RN1-6	4	30/138		IJ	P
RC-Moukondo-RN1-7	1	22/110	22/110	IX	P
RC-Moukondo-RN1-8	1	09/124	09/124	IX	P
RC-Moukondo-RN1-9-a	2	15/128	12/088	ID	P
RC-Moukondo-RN1-9-b	2	32/254	30/275	IS	P
RC-Moukondo-RN1-10-a	2	22/110	22/110	IX	P
RC-Moukondo-RN1-10-b	2	32/290	32/290	IX	P
RC-Moukondo-RN1-11-a	2	09/124	08/104	ID	P
RC-Moukondo-RN1-11-b	2	32/280	32/287	IS	P
RC-Moukondo-RN1-12-a	2	11/132	11/115	ID	P
RC-Moukondo-RN1-12-b	2	32/290	32/297	IS	P
RC-Moukondo-RN1-13-a	2	15/119	13/085	ID	P
RC-Moukondo-RN1-13-b	2	32/254	31/272	IS	P
RC-Moukondo-RN1-14-a	2	20/119	18/091	ID	P
RC-Moukondo-RN1-14-b	2	32/260	31/279	IS	P
RC-Moukondo-RN1-15-a	2	10/124	08/084	ID	P

Legend	Meaning
MJ	Mouvement plane with extension
NS	Sinistral plane with extension
IS	Sinistral plane with reverse component
ID	Dextral plane with reverse compnent
DJ	Dextral plane with extension
TJ	extension fracture
XX	Unknown sense of mouvement
P	Probable sens of mouvement
C	Certain sens of mouvement
S	Supposed sens of mouvement

Type of structure	Meaning
1	Fault with striae
2	Conjugate fault
3	Shear plane with extension fracture
4	Fracture with mouvement

Table S1. Data on earthquake focal mechanism solution used for stress inversion in this study. The focal mechanism solution data were compiled only from several literature review, Global CMT moment tensor, and GFZ GEOFON earthquake catalogs.

EVENTID	DATE(dd/mm/yr)	TIME	LAT	LON	TYPE	MAG	DEPTH	Strike	Dip	Rake	Reg	R'	Shmax	Shmin	Region	Author
111881A	18-11-81	09:17:34	-2,46	22,81	mw	5,5	10	226	84	-156	SS	1,5	90	0	DRC	Harvard CMT
WA191181	19-11-81		-2,83	22,767	mb	5,6	8	238	86	-171	SS	1,5	103	13	DRC	Suleiman et al, (1993)
012687A	26-01-87	23:11:52	7,85	12,95	mw	4,9	15	174	27	60	TF	2,5	100	10	Cameroon	Harvard CMT
092295D	22-09-95	08:51:57	1,12	19,51	mw	5,3	15	315	32	116	TF	2,5	30	120	DRC	Harvard CMT
030598B	05-03-98	02:59:52	1,38	17,04	mw	5	15	151	33	96	TF	2,5	58	148	Republic of Congo	Harvard CMT
042698C	26-04-98	14:16:58	0,64	17,4	mw	5,2	15	165	26	132	TF	2,5	53	143	Republic of Congo	Harvard CMT
WA980305	05-03-98	02:59:43	0,81	17,42	mb	5,4	10	151	49	71	TF	2,5	75	165	Republic of Congo	Ayele (2002)
WA980426	26-04-98	14:16:52	0,86	17,34	mb	5,5	6	209	55	138	TS	2	87	177	Republic of Congo	Ayele (2002)
WA950922	22-09-95	08:51:50	1,07	19,4	mb	5,6	15	106	62	75	TF	2,5	31	121	Republic of Congo	CMT (Dziewonski et al.,1996)
201912191525A	19-12-19	15:26:02	1,67	8,31	mw	5,5	31,6	173	50	170	TS	2	40	130	OFF S, COAST OF NORTHWES	Harvard CMT
WA191219	19-12-19	15:25:59	1,76	8,18	mw	5,5	29	171	49	167	TS	2	40	130	OFF S, COAST OF NORTHWES	Geofon
202005211257A	21-05-20	12:57:37	-9,36	24,01	mw	4,9	41,7	67	31	113	TF	2,5	145	55	DRC	Harvard CMT
202008041144A	04-08-20	11:44:07	-5,39	22,87	mw	4,7	17,3	225	79	178	SS	1,5	90	0	DRC	Harvard CMT
202103061708A	06-03-21	17:08:57	-1,01	10,34	mw	5	12,7	204	46	-73	NF	0,5	12	102	Gabon	Harvard CMT
202103092307A	09-03-21	23:07:58	-0,95	10,35	mw	5,3	12	351	43	113	TS	2	121	31	Gabon	Harvard CMT
WA090321	09-03-21	23:07:46	-1	10,36	mw	5,3	10	200	44	-62	NF	0,5	2	92	Gabon	Geofon
WA060321	06-03-21	17:08:56	-1,12	10,24	mw	5	10	189	54	-92	NF	0,5	10	100	Gabon	Geofon
WA91245	09-12-45		2,276	10,9	mm	6,1	11	18	82	-180	SS	1,5	63	153	Gabon	Suleiman et al, (1993)
WA740923	23-09-74		-0,283	12,808	mw	6,1	3	344	41	86	TF	2,5	77	165	Gabon	Foster and Jackson (1998)
WA220639a	22-06-39	22:19:09	5,18	-0,13	mb	6,8	15	350	90	0	SS	1,5	125	35	Ghana	Yarwood et Doser (1990)
WA220639b	22-06-39	22:19:09	5,18	-0,13	mb	6,8	15	60	90	0	SS	1,5	15	105	Ghana	Yarwood et Doser (1990)
WA220639c	22-06-39	22:19:09	5,18	-0,13	mb	6,8	12	350	86	3	SS	1,5	16	106	Ghana	Suleiman et al, (1993)
WA220639d	22-06-39	22:19:09	5,18	-0,13	mb	6,8	15	61	88	5	SS	1,5	125	35	Ghana	Suleiman et al, (1993)
WA221283a	22-12-83		11,98	-13,54	mm	6,6	11	95	80	-160	SS	1,5	138	48	Guinea	Suleiman et al, (1993)
WA221283b	22-12-83		11,98	-13,54	mm	6,4	12	90	60	-160	SS	1,5	130	40	Guinea	Dorbath et al, (1984)
WA190305	19-03-05	11:49:18	4,18	11,02	mw	4,6	8	230	89	7	SS	1,5	5	95	Cameroon	Ngatchou et al, (2018)
WA150576a	15-05-76	08:09:57	4,46	19,35	mw	5,6	23	250	55	152	TS	2,5	130	40		Fairhead and Stewart, (1983)
WA150576b	15-05-76	08:09:57	4,463	19,363	mm	5,5	12	134	19	86	TF	2,5	46	136		Suleiman et al, (1993)
WA300971a	30-09-71		-0,45	-4,89	mm	5,9	12	63	57	50	TF	2,5	1	91	Gul of Guinea	Suleiman et al, (1993)
WA300971b	30-09-71		-0,45	-4,89	mm	5,9	13	72	60	60	TF	2,5	6	96	Gul of Guinea	Lui and Kanamori, (1980)

Seismogenic Fault Reactivation in Western Central Africa: Insights from Regional Stress Analyses

Hardy Medry Dieu-Veill Nkodia[1], Timothée Miyouna[1], Folarin Kolawole[3,4], Florent Boudzoumou[1,2], Alan Patrick Rodeck Loemba[1], Nicy Carmel Tchiguina Bazebizonza[1], Damien Delvaux[5]

[1]Marien NGOUABI University, Faculty of Sciences and Technics, Department of Geology, B.P. 60, Brazzaville, Republic of Congo.
[2]National Research Institute in Exact and Natural Sciences of Brazzaville, P.O. 2400, Republic of Congo (IRSEN).
[3]Lamont-Doherty Earth Observatory, Columbia University, 61 Rte 9W, Palisades, NY, United States.
[4]BP America, 501 West Lake Blvd., Houston, TX, United States.
[5]Department of Geology, Royal Museum for Central Africa, Leuvensesteenweg 13, B-3080 Tervuren, Belgium.

Corresponding author: Hardy Medry Dieu-Veill Nkodia[1] (nkodiahardy@gmail.com).

Key Points:

- A transpressive regime with NNE-SSW horizontal maximum compressive stress controls intraplate seismicity in Western Central Africa
- Regional stresses acting on offshore oceanic fracture zones are compatible with those acting along the onshore continental margin.
- Favorable orientation and hydrothermal alteration of onshore preexisting Archean - Cenozoic faults make them susceptible for reactivation.

Abstract

The onshore continental margins of western Central Africa have been hosting potentially damaging earthquake events for decades; yet, the links between the seismicity, the contemporary stress field, and pre-existing faults are not well understood. Here, we analyze the regional stress fields along the coastal margin and interior cratonic areas using earthquake focal mechanisms, map and characterize the detailed structure of preexisting fault systems in outcrops, and asses the reactivation potential of the mapped structures. Our results show that the earthquakes originate under a transpressive stress regime with a horizontal maximum principal compressive stress ($\sigma 1$) that is oriented NNE-SSW. We show that regional stresses acting on offshore oceanic fracture zones are compatible with those acting along the onshore areas of the continental margin. Field observations reveal the presence of large fault systems that deform both the Precambrian basement and Phanerozoic sedimentary sequences, with widespread hydrothermal alterations of calcite veining, quartz veining, and palygorskite mineralization along the fault zones. Along the margin, the preexisting NNE-, NNW-, and N-S -trending strike-slip faults and normal faults show a high slip tendency (60 – 100 %), whereas in the cratonic interior, the NW- and N-S -trending thrust faults are the most likely to reactivate. We argue that favorable orientation of the preexisting faults and potentially, their hydrothermal alteration products, define the susceptibility of the faults to seismic reactivation. We propose that possible stress propagation into the near-shore and onshore tip zones of oceanic fracture zones may be driving stress loading on pre-stressed fault systems onshore.

Keywords: Earthquakes, Intraplate seismicity; Slip tendency; faults; Western Central Africa; focal mechanism.

Plain Language Summary

We investigated the stresses that are generating earthquakes and the compatibility with preexisting fault systems along the stable continental margin of Western Central Africa. The stresses acting on the continent interior were also determined and distinguished. We found that the regional stresses acting on offshore oceanic fracture zones are compatible with those acting along the onshore areas of the continental margin. In this stress field, the potential for reactivation of the observable preexisting onshore fault systems is very high, particularly for those oriented NNE-SSW and N-S. We propose that the stresses along transform faults and oceanic fracture zones may propagate into near-shore and onshore areas, leading to earthquakes on the preexisting faults.

1 Introduction

Earthquakes remain one of the most catastrophic natural hazards in human history. Beyond the associated fatalities, earthquakes also leave behind lasting environmental and economic crises in the affected communities. Although, the largest magnitude earthquakes have been recorded along plate boundaries (McCaffrey, 2008) associated with plate subduction, collision, and continental rifting, several large magnitude (Mw>6) events have also been recorded in intraplate regions (e.g.,Talwani, 2014; Tuttle et al., 2002), and more intriguingly, along passive continental rift margins where the sources and occurrence of earthquakes remain less understood. Among the large magnitude and devasting earthquakes recorded in continental intraplate regions previously thought to be relatively stable include the Mw 6.2 Latur Earthquake of September 29, 1993 in South India which claimed a death toll of 11,000 (Gupta et al., 1998) and the Mw 6.2 Guinea earthquake of December 22, 1983 which caused 1500 fatalities and significant property damage (Musson, 1992; Suleiman et al., 1993). On the causes of intraplate seismicity, proposed hypotheses include the reactivation of preexisting structures (e.g., Calais et al., 2016; F. Kolawole et al., 2019; Folarin Kolawole et al., 2017; Ngatchou et al., 2018) driven by far-field stress transmission from active plate boundaries (Delvaux et al., 2016; Delvaux & Bath, 2010; Nkodia et al., 2020; Wiens & Stein, 1983, 1985), gravitational body forces (Levandowski et al., 2017), deglaciation-related isostatic rebound (Lund Snee & Zoback, 2020), underground industrial activities(Grigoli et al., 2017; Keranen & Weingarten, 2018) , and thermal weakening of the lithosphere (Holford et al., 2011). Some passive rifted margins across the world are known host pronounced distributed seismicity, among which are well-instrumented regions such as the eastern Brazilian Atlantic margin (Assumpção, 1998), the southern Australian margin (Holford et al., 2011), and the eastern North American margin(Sbar & Sykes, 1973; Zoback, 1992). However, in poorly instrumented regions, such as Equatorial West Africa and western Central Africa where widespread seismicity is becoming increasingly prominent, the relation between the present-day stress regime acting in these regions, the sources of stress perturbation, and the mechanics of reactivation of inherited structures are not known (Olugboji et al., 2021) . This knowledge gap hinders the development of viable early-warning mechanisms for hazard mitigations in local communities located in such regions.

In this study, we explore the passive margin of Western Central Africa, an area which exemplifies considerable intraplate seismicity in both its offshore domains and within the continent (Figs. 2a-b). This region has been the subject of much research for almost a century (Krenkel, 1923; Junner and Bates, 1941; Blundell, 1976; Burke, 1976; Bacon and Quaah, 1981; Ambraseys and Adams, 1986; Yarwood and Doser, 1990; Onuoha and Ezeh, 1992a; Musson, 1992; Suleiman et al., 1993; Delvaux and Bath, 2010; Amponsah et al., 2012; Kutu, 2013; Nwankwoala and Orji, 2018; Meghraoui et al., 2019; Oladejo et al., 2020; Olugboji et al., 2021; Kadiri and Kijko, 2021). Although most of the studies focused on the use of remote sensing to provide a seismotectonic model for the region (Adepelumi et al., 2008; M. O. Awoyemi et al., 2017; M. Awoyemi & Onyedim, 2004; Bouka Biona & Sounga, 2001; Oladejo et al., 2020), the characterization of the structures is sparse, and there remains a limited understanding of the detailed structure and current stress state of the potentially-seismogenic preexisting faults.

The aim of this contribution is to evaluate the possible current regional stress regime that is most dominant and is responsible for reactivating preexisting structures along the western Central African passive margin by using the slip tendency analytical techniques. By determining which types of structures that are being reactivated within the study area and the associated kinematics, we provide some insight into the seismic hazards and possible drivers of widespread seismicity along the margin. We suggest that the results of this study are relevant for building a realistic model for seismic hazards and the associated coseismic ground motions for this region and similar poorly-instrumented passive margin environments:

2 Geological and Tectonic Setting

2.1 Regional Geology of Western Africa and Continental Margin

The Western Africa continental region is mainly dominated by Archaean basement, overlain by Neoproterozoic and Phanerozoic units (Fig. 1). The Archean rocks are hosted within the Congo Craton in the western Central Africa region and in the West African Craton in the far northwestern sub-region. These cratons are separated into several blocks limited by Neoproterozoic and Paleoproterozoic terranes and shear zones, interspersed by sedimentary basins (Fig. 1). The 3.1 - 2.7 Ga Congo Craton (Thiéblemont et al., 2009; Turnbull et al., 2021) is subdivided into five blocks: (i) the Ntem-Chaillu block in the central and northwestern domains, covering the region of Cameroon, Gabon, and Republic of Congo (Kessi, 1992; Tchameni et al., 2000; Gatsé Ebotehouna et al., 2021a); (ii) the 2.5 Ga Angola block to the south in Angola (De Carvalho et al., 2000; Jelsma et al., 2018); (iii) the 3.6 - 2.5 Ga Kassaï block to the southeast in DRC (Batumike et al., 2006); (iv) the 3.2 - 2.5 Ga NE-Congo Block in the Northern DRC (Turnbull et al., 2021), and (v) the 2.8 - 2.6 Ga Tanzanian block.

These cratonic blocks have accommodated multiple episodes of large-scale brittle deformation which emplaced large discontinuities within them. Akame et al., (2020, 2021) documented the presence of large NW-SE, NE-SW and E-W trending brittle and ductile shear zones in the Ntem-Chaillu Block, inherited from Neoarchean orogenesis. Similar deformation were also reported in the laterally equivalent Souanké Archean rocks in the Ivindo region of Republic of Congo (Loemba et al., 2022) In the Souanké domain, the brittle shear zones show evidence of reactivation into normal faulting kinematics interpreted to be related the Cretaceous opening of Atlantic Ocean (Loemba et al., 2022).The Ntem-Chaillu block is bounded to the north by the Oubanguides Belt which developed during the Pan-African Orogeny (550 ±100 Ma) and was subsequently deformed in the Mesozoic by the continental-scale, NE-trending Central African Shear Zone (CASZ; Fig. 1). The CASZ, which extends into the Borborema province of NE Brazil (Miranda et al., 2020), is considered to be an accommodation zone that was activated during the opening of the South Atlantic (Moulin et al., 2010; V. Ngako et al., 2003; Vincent Ngako et al., 1991; Njonfang et al., 2008; Wilson, 1965). Recent earthquakes and associated source mechanisms along a segment of the CASZ (e.g., 2005 Montalé, Cameroon earthquake) suggests that the CASZ structure may still be active as the Atlantic Ocean basin continues to open (Ngatchou et al., 2018).
Along the western margin of the Congo Craton, the Ntem-Chaillu and Angola cratonic blocks are separated by the Pan-African West-Congo Belt (630 Ma – 490 Ma) the western part of which was later rifted during the opening of the Atlantic Ocean (Alvarez & Maurin, 1991; Boudzoumou & Trompette, 1988; Bouenitela, 2019; Fullgraf et al., 2015; Hossié, 1980). The fold-thrust terranes of the West-Congo Belt is noted to host large (>90 km-long) NE-SW, NW-SW and N-S trending brittle shear zones (Alvarez & Maurin, 1991; Nkodia et al., 2021). In the Republic of Congo (RC), Democratic Republic of Congo (DRC), and Angola, the terranes of the mobile belt are covered by Ordovician-Silurian sandstones which record phases of strike-slip deformation, first during the Gondwanide Orogeny in the Permo-Triassic, then during Cretaceous opening of the Atlantic

(Miyouna et al., 2018; Nkodia et al., 2020). The Late Paleozoic sandstones of the Inkisi Group show reactivated and segmented strike-slip faults zones oriented NW-SE, NE-SW, and E-W, observable in field outcrops (Miyouna et al., 2018; Nkodia et al., 2020a) and in seismic reflection images (Damien Delvaux et al., 2021; Kadima et al., 2011). The phases of Late Paleozoic-Early Mesozoic contractional tectonic deformation in the Congo Basin are observable across eastern and southern Africa (Delvaux et al., 2021) However, there is evidence for the presence of through-going structures which deform both the Paleozoic-Mesozoic and Cenozoic sedimentary sequences (Damien Delvaux et al., 2021; Kadima et al., 2011), suggesting there might be still be on-going intra-continental tectonic deformation in Central Africa. Mbéri Kongo (2018) showed that the Paleogene sand deposits of the Bateké Plateau, Congo Basin, have been deformed by large strike-slip faults with associated conjugate normal faults. Northwest of the Oubanguides Belt, in West Africa, the Cretaceous intracratonic Benue Rift developed within the Trans-Sahara Mobile Belt as a corridor of transtensive faults with associated magmatism (Ajakaiye et al., 1986; Benkhelil, 1989; Oha et al., 2020). The closure and failure of the rift occurred in the Santonian, associated with a transpressional deformation of its Cretaceous syn-rift deposits (Ofoegbu, 1985; Benkhelil, 1989). The Trans-Sahara Mobile Belt host several N- to NNE-trending shear zones associated with the Proterozoic amalgamation of West Gondwana. Some of the shear zones also record evidence of brittle deformation during the opening of the Atlantic Ocean, an example of which is the Kandi fault zone which served as an accommodation zone during the rifting event (Affaton et al., 1991).

Figure 1: *Map of the bedrock geology of the Nubian Plate showing major litho-tectonic subdivisions of the crust. Dwc1, Dk, Dbk, Dngov, Dso represent field sites where structural measurements of fault systems were collected. Dwc1 represent the study site of a thrust fault system in western Congo. Dwc2 is a combination of strike-slip faults along Dk and Dngov which represent field sites in Kolas Quarry, Republic of Congo, and Ngovo Cave, Democratic Republic of Congo respectively. Dbk represents the field study sites of fault systems in Brazzaville and Kinshasa areas. AFZ: Akwapim Fault Zone, BFZ: Bouandary Fault Zone, CASZ: Central African shear zone.*

2.2 Oceanic Fracture Zones in the Gulf of Guinea, Western Nubian Plate

The oceanic crust of the Atlantic Basin dominates the western portion of the Nubian Plate and hosts several fracture zones that extend eastward from the active transform faults at the Mid-Atlantic Ridge plate boundary towards western Africa's rifted continental margin (Fig. 1). Oceanic transform faults developed within the oceanic crust starting sometime after continental break-up and serve to accommodate the lateral movement of tectonic plates, and lateral variation of spreading rates, and to facilitate connectivity between ridges and trenches (De Long et al., 1977, p. 199; Gerya, 2012; Hensen et al., 2019). Due to their strong topographic expression at the sea floor , their structural and geochemical alteration of the oceanic crust, and temporal accretion patterns, transform faults and oceanic fracture zones are mappable in bathymetric, seismic reflection, gravity, and magnetic datasets (Delteil et al., 1974; Fail et al., 1970; Gorini & Bryan, 1976; Guiraud et al., 2010; Mascle & Sibuet, 1974).

Although the active plate boundary (i.e., spreading oceanic ridges and subduction zones) host most of the seismicity of oceanic basins, oceanic fracture zones and their flanking areas also accommodate significant seismic activity and represent seismic hazards within intraplate areas away from the plate boundaries (Fig.2a; Burke, 1969; Lay, 2019; Okal & Stewart, 1982). On the lateral growth of oceanic fracture zones, Burke et al. (1969) proposed a mechanism of propagation towards the continents by extension fracture mode which produce stress transmission that initiate seismic failure at the continental margins. In the Atlantic Ocean, some of the most active fracture zones which commonly extend close to- or into the western Africa rifted continental margin include Romanche, Chain, Charcot, Ascension, and Saint Paul fracture zones (Figs. 2a-b; Heezen et al., 1964, 1965; Mascle & Sibuet, 1974). A few studies argue for the lateral continue of oceanic fracture zones onto the continent of West Africa and causative relationship with onshore earthquakes based on: 1) the alignment of on-shore magnetic lineaments in Nigeria with the trends of the offshore fracture zones (Ajakaiye et al., 1986), and 2) the colocation and alignment of rifted transform margins such as the Ghanian and Ivorian coastline with the Romanche and St Paul fracture zones respectively (Fig. 2a; Antobreh et al., 2009), and 3) recent (<10 million years) acceleration of strain rates on oceanic transform faults post-continental break-up in the Late Cretaceous (Meghraoui et al., 2019). However, questions remain on the link between the current stress regime acting on the margin of western African continent and the mechanisms and triggers of seismic reactivation of preexisting structures.

3 Data and Methods

3.1 Earthquake Data

The study area covers the region between latitudes 16.70°N and 14.07°S, and longitudes 23°W and 24.66°E. For this region, we built a database of earthquakes and their related focal mechanism data from publicly-accessible global catalogues which includes the International Seismic Center (ISC), the United States Geological Survey (USGS), the Global Centroid-Moment-Tensor (CMT), and the GFZ GEOFON earthquake catalogs.

3.2 Mapping of Tectonic Lineaments

In order to delineate mega-scale tectonic structures in the oceanic crust and around the onshore continental coastal margin, we utilized hillshade digital elevation model (DEM) maps generated from bathymetric and topographic data. In the offshore areas, we delineated and mapped the traces of oceanic fracture zones on DEM of bathymetric data extracted from GEBCO (GEBCO Bathymetric Compilation Group 2021, 2021), which has a spatial resolution of 1 arc minute (~1.5 km). Within the onshore continental areas, using previously published geologic maps and field observation where possible (see details in section 3.3) as constraints, we manually interpreted and digitized visible structural lineaments defined by steep laterally-continuous topographic relief gradients from a mosaic of scenes of a 30 m resolution ALOS-type radar interferometric digital elevation model (DEM) images, following a standard approach (Burbank & Anderson, 2011). The ALOS data was obtained from the ALOS Global Digital Surface Model (https://www.eorc.jaxa.jp/ALOS/en/aw3d30/data/index.htm). The previously published geologic map that guided the lineament interpretation is the tectonic map of Africa by Milesi et al. (2010) in which the faults were compiled from field studies and gravity anomalies, conducted by geological surveys groups of different countries.

3.3 Field Observations and Collection of Structural Measurements

In the onshore areas of the Republic of Congo (R.C) and Democratic Republic of Congo (D.R.C), we conducted field observations and collection of structural data along the fault and fracture systems in outcrops. This field campaign also served as ground-truthing to constrain the mapping of structural lineaments in hillshade maps. The field campaigns were conducted in the regions of Brazzaville, Dolisie, and Souanké regions of R.C, and in the Kongo Central region of D.R.C. The fieldwork helped to confirm the geologic origin of some of the interpreted lineaments as fault strands or brittle shear zones where they are accessible. In the field outcrops of the faults and brittle shear zones, we collected measurements of strike and dip of fault planes, trend and plunge of slip vectors (striations) along the surfaces, and we documented evidence and characteristics of geochemical alterations of the fault zones. We have provided information on our field measurements in the supplementary file of this manuscript. The structural field measurements provide fault plane orientation data that we used as one of the inputs into the slip tendency analysis (see section 3.4).

3.4 Assessment of Contemporary Stress Field and Slip Tendency of the Preexisting Structures

Following a standard approach, we used the Win-Tensor program (D. Delvaux, 2012) to determine the current stress field acting on the Gulf of Guinea section of the Nubian Plate, using the information on source parameters of earthquake focal mechanism solutions as input data. The focal mechanism solution data were compiled from several literature review (see supplementary files), Global CMT moment tensor, and GFZ GEOFON earthquake catalogs (Fig. 2b). In cases where the focal mechanism solution of the same earthquake event is produced by multiple earthquake databases, we considered all the solutions in order to guarantee the precision of the resulting stress tensor solutions. For our analysis, since the available focal mechanism solutions are sparse across the region and the seismicity is distributed across 1) offshore and onshore areas along the coastal margin corresponding to a rifted tectonic domain and the underlying pre-rift Proterozoic mobile belt, and 2) an Archean cratonic interior that has experienced failed rifting and inversion, we divided the study region into three sub-regions defined by three boxes (sub-regional Boxes 1, 2, and 3 in Fig. 3b). The division was made by considering the assumption that each box has a uniform stress. Two boxes cover the coastal margin areas: one along the Gabon-Cameroon and the other along the Ghanian coastal margins; whereas the third box covers the cratonic continental interior of central Africa.

The Win-Tensor program uses the stress inversion method (Angelier, 1975, 1989; Angelier & Mechler, 1977) to determine a reduced tensor which contains the orientations of the principal compressive stress axes ($\sigma 1$, $\sigma 2$, and $\sigma 3$) and the stress ratio, R. The program first estimates the tensor solution using the determination of PBT (compression, intermediate and tensional) axes method and the Right Dihedron method. This initial stress tensor solution serves as a starting point to determine a more constrained tensor solution using an iterative Rotational Optimization method. The latter method uses a misfit function that minimizes the difference between the calculated slip direction and the resolved direction. Fault planes that show large misfit angle are rejected in order to have a better constrained result. The stress index regime, R', typified the regime associated with the solution tensor. R' is an improved R ratio that gives the type of stress regime in a continuous scale of 0 to 3 (Fig. 2).

Figure 2: *Standard values of the stress index R' with respect to the stress regime (modified from Delvaux et al., 2017).*

The resultant tensor solutions from Box 1 and Box 2 were applied on the mapped fault systems in central Africa to determine the slip tendency of the different observed fault plane geometries. Note that we do not use the tensor solution for Box 3 because it is similar to that of Box 1 (see section 4.3). Slip tendency quantifies the potential for reactivation of fault planes under a given stress field (Morris et al., 1996). The magnitude of slip tendency depends on the ratio of shear stress to normal stress resolved on a fault or fracture surface, and the frictional characteristic of the rocks. The Win-Tensor program determines a normalized slip tendency (Tsn) (Lisle & Srivastava, 2004) rendered as continuous values in a colored scale of 0 to 1. The planes with a slip tendency above 0.6 are considered to have a high likelihood to be reactivated, and less likely are the planes below 0.6. For our analysis, we use 0.3 as the coefficient of friction according to the work of Angelier (1989). We assume a cohesionless residual strength envelope for the faults, defined by 0 MPa cohesion, based on the outcrop observation of widespread brittle reactivation of hydrothermally-altered fault zones (see section 4.2).

4 Results

4.1 Spatial Distribution of Earthquakes and Mapped Tectonic Lineaments

Offshore, seismic events are either collocated with or occur in the vicinity of traces of oceanic fracture zones which show dominant trends of ENE and NE (Fig. 3a). Some events also occur along the Cameroon volcanic line and around the Bi**é** Dome in Angola. However, onshore, along the coastal margin and continental interior areas, the regional seismicity patterns show clustering of events that are collocated with or in vicinity of the mapped tectonic lineaments (Fig. 3a). For example, at the location of field site Dso, the epicenter of a Mw 6 event is collocated with the trace of a large ENE-to-NE trending fault system in the Ntem-Chaillu Block (see lineament with label 'Dso' in Figs. 1 and 3a). More interestingly, earthquakes cluster at the location where the Romanche Fracture Zone extends onto the Ghanian shoreline (Fig. 3a); and at least one of each of the nodal planes on the associated focal mechanism solutions show a trend that is parallel or sub-parallel to the fracture zone orientation (Fig. 3b). In southern Ghana and surrounding regions, tectonic lineaments show dominant sets trending NNE and ENE of which the latter is parallel to the trend of the Romanche Fracture Zone (Fig. 3a). Most of the focal mechanism solutions of the earthquakes (Fig. 3b) show a dominance of thrust fault and strike-slip fault regime. Only 10 % of events show normal faulting regimes (pie chart in Fig. 3b) and most are restricted to the rifted costal margin. Within the continental interior, the strike-slip and reverse faulting regime appear to be distributed across a broad region.

Figure 3: *(a) Relief map showing the distribution of earthquakes in the Western Africa passive margin. AFZ, CASZ are the Akwapim Fault zone, the Central Africa shear zone. (b) Focal mechanism solutions for earthquakes in the western part of the Nubia Plate, obtained from several literature review, Global CMT moment tensor, and GFZ GEOFON earthquake catalogs. The boxes show the area where conducted stress inversion on focal mechanism results. The pie-chart show the frequency distribution of the different tectonic regime acting on the area. TS: trenstensional regime; NF: normal faulting regime; SS: strike-slip faulting regime; TF: thrust faulting regime.*

4.2 ***Fault Structure in the Field Outcrops***

The study area is dominantly affected by strike-slip faults trending NW-SE, NE-SW, and minor ENE-WSW to E-W. Locally, these regions showed thrust faults and normal faults settled during Pan-African orogenies, post-Pan-African and the opening of Atlantic Ocean. At the field sites in Republic of Congo (RC) and Democratic Republic of Congo (DRC), observable deformation in the Paleozoic sandstones of the Inkisi Group mostly showed steep strike-slip faults and joints. Almost all strike-slip faults are arranged in relay segments or in a corridor of segments connected by extension fractures (Figs. 4a, 4d). Their traces attain 400 m in length in the outcrops, but their corresponding lineaments mapped in regional-scale DEM hillshade maps reach 80 - 90 km. In quarries, cross-sectional views of the fault-fracture systems show exposures of up to 50 m in height.

The fold-thrust terrane of the West Congo Belt is composed of two domains with distinct structural styles. One of the domains is dominated by major NW-trending low- to high-angle thrusts which control the NE vergence of the belt, and their associated high-angle back-thrusts (Fig. 4b). This structural style primarily affected schistose rocks with intruded dolerite, diamictites, quartzites, and sandstones units. The other domain is marked by a basin structure, a synclinorium, that rest on thrust sheets within the orogenic belt. This basin is dominated by carbonate sequences which are cut by major NE-trending strike-slip brittle shear zones (Fig. 4e). The strike-slip shear zones are arranged in step-overs associated with én-echelon extension fractures or normal faults. These faulting styles are observable down to 200 m depths in the caves of Ngovo and Ndimba. In northern RC, Archean rocks of Souanké host 2.8 Ga charnokites, gneisses, and pegmatites which are also deformed by the brittle shear zones. Nearly all the brittle shear zones observed on the field show linking architecture with relay zones connected either by extension fractures or duplex structures (Fig. 4c). On a slip surface along the strike-slip faults, we find evidence of over-printing of sub-horizontal slickenlines by vertical slicklines (Fig. 4f), indicating that these NE-SW, WNW-ESE, NW-SE and N-S trending strike-slip faults have been reactivated in dip slip.

Figure 4: *Field observations of faults systems. (a & d) Fault systems in outcrops of the Inkisi Group (Dbk), showing fracture patterns (highlighted in white dashed line in 3a), and a fault zone showing segmented faults in a duplex zone (in 3d), at the Kombé quarry, located near the Congo River, Brazzaville. (b & e) Faults systems (Dwc1 & Dk) in the West-Congo Belt showing successively thrust and back-thrust affecting schists and quarzites, in Dolisie along the RN1 primary road, and strike-slip fault planes in Kolas quarry near Loutété region. (c & f) Faults systems (Dso) in Souanké showing high-angle planes of strike-slip faults in the area (in 3c) and, a NE-trending plane that shows horizontal striae that is over-printed by vertical striae associated with calcite fibers, indicating a later normal faulting reactivation of the strike-slip faults. The dashed lines in Fig. 3f represent the directions of striae.*

In addition to the observed brittle deformation along the fault systems, we also note a widespread occurrence of geochemical alterations along the fault zones. For example, at field sites Dwc1 and Dk located in the West Congo Belt, several strike-slip fault zones show calcite mineralization that occur in accretion steps (Figs. 5a-c), and a few other fault zones show iron staining along the fault planes (Fig. 5b,c,d). Likewise, in the fault zones hosted in schistose terranes (e.g., Dk and Dngov), we observe networks of quartz veins injected along thrust faults and shear zones (Fig. 5f). In the sedimentary sequences (Inkisi Group; location Dbk), the fault zones are either mineralized by palygorskite, calcite, or a mix of both (Fig. 5e). However, at all the field sites visited, we commonly observed brittle reactivation of the mineralized fault and fracture planes evidenced by sheared mineral fibers with characteristic chatter marks, or tensile fracturing of the mineralized zones.

Figure 5: *Geochemical alterations along mineralized fault surfaces. (a) Accretion calcite steps along NW-SE strike-slip faults in carbonates rocks of the West Congo Belt, DRC. (b - c) Carbonate-hosted faults surfaces covered by accretion calcite steps and iron staining. Note that the carbonate rock in Figure 5b has penetrative cross-bedding structures that should not be confused with slickenlines. (d) Fault surface in Inkisi sandstones associated with iron alteration realm. (e) Slickensided palygorskite along a fault in Dbk fault system. (f) Deformed doleritic intrusion along a high-angle thrust fault (230/40) injected with quartz veins in the Dwc1 faults system.*

4.3 Contemporary Stress Fields within the Analyzed Sub-Regions

All three sub-regional boxes show a compressional strike-slip (i.e., transpressive) stress regime with a maximum horizontal compressive stress (SHmax) orientation that lies in the NE-SW quadrant (Fig. 6). The quality of tensor solutions is of B type, indicating that they are well-constrained. The standard deviation of the Shmax is less than ±15° for all the boxes, as Box 1, 2, and 3 show Shmax standard deviations of ±5.7, ±11.1, and ±14.3 respectively. The nodal planes of all tensors are in reactivated positions in the Mohr diagram (Figs. 6c, d, f). However, unlike the Box 2 where SHmax is oriented NE-SW (051° trend, 30° plunge), boxes 1 and 3 are more similar in that they show an Shmax orientations of NNE-SSW (014° trend, 4° plunge) and N-S (184° trend, 3° plunge) respectively. In a transpressive stress regime, the SHmax corresponds to the maximum principal compressive stress ($\sigma 1$).

Both Boxes 1 and 3 show strike-slip nodal planes that are oriented NW-SE and NE-SW (Figs. 6b, 6b-e); however, Box 1 has events with E-W trending sinistral and high-angle N-S trending normal nodal planes, and in Box 3, some of the events show conjugate reverse faulting patterns with nodal planes trending NW-SE and ENE-WSW. In Box 2, most of the nodal planes show high-angle and low-angle reverse faulting, and some of the high-angle reverse nodal planes show an obliquity associated with a secondary strike-slip motion. Boxes 1 and 2 yield index R' values of 1.75 and 1.85 (Table 1), indicating that both sub-regions are undergoing a transition between pure strike-slip and compressional regimes. Whereas, in the continental interior in Box 2, the inversion shows an index R' of 2.2, suggesting a more dominant compressional regime and less prominent strike-slip regime.

Figure 6: *Results of stress tensors from the inversion of earthquake focal mechanism solution along the western Africa continental margin, offshore and onshore Gulf of Guinea represented by sub-regional boxes (see Fig, 3b).*

Table 1: *Stress parameters associated with the focal mechanism solution of earthquakes in Box 1, Box 2, and Box 3 in Figure 2b. n: number of data used, nt: total data, Pl & Az: plunge & azimuth of principal compressive stress tensors, R': index regime; Reg: Regime, QRfm: Quality rank of focal mechanism.*

4.4 Slip Tendency of Preexisting Fault systems

The application of stress tensors of Box 1 and Box 2 to the fault systems mapped onshore along the coastal margin (i.e., Box 1 sub-region) show that several faults that are more likely to be reactivated if the dominant stress field is that of Box 1 (transpressive with NNE-SSW SHmax; Figs. 7a,c,e,g & 8a,c,e,g). This sub-region covers the Archean rocks of Souanké, the West Congo Belt, and approximately the Inkisi Group. The NNW- and NNE-oriented planes of strike-slip faults showed the highest values of TsN = 80 to 100 %. Also, we note that some of the NNE- and NE-trending normal faults are in a position of reactivation as they show TsN values of >60 %. Here, the WNW- to E-W -oriented faults show the lowest values of TsN, suggesting they could not be reactivated in such stress field. The WNW- to E-W planes are mis-oriented for reactivation as they plot beneath the failure envelope (residual strength envelope) in the Mohr diagram (see blue circles in Figs. 7c, d, g, h & 8c, d, g, h). Overall, the Mohr diagram for the Box 1 regime test indicate that most of the faults are in a position of reactivation.

Whereas, assuming the Box 2 stress field (transpressive with NE-SW SHmax; Figs. 7b, f & 8b, d), very few faults are at failure, suggesting a significantly lower likelihood of reactivation. The possibility of reactivation of the mapped strike-slip faults and normal faults in the Box 2 stress regime is less probable as most of the TsN values are <60 %. Only thrust faults in the West Congo Belt are likely to be reactivated and particularly, the back-thrusts. In Box 2 stress regime, most of thrust faults show TsN values >60%. However, there are a few thrust faults that are in the position of reactivation in the Box 1 stress regime; for example, a major thrust fault system that is associated with the vergence of the orogenic belt (Fig. 8b). Also, in the Box 2 stress regime, the major NE-oriented planes are fault systems that couldn't be reactivated as they plot beneath the failure envelope in the Mohr diagram.

Figure 7: *The application of the stress inversion results for Box 1 (left column) and Box 2 (right column) on Dbk and Dso fault systems and the resulting Slip Tendency values associated with their Mohr-Coulomb stress states. The slip tendency estimate associated with each fault segment is presented as color-coded planes in both the stereoplots and their adjoining Mohr diagrams*.

Figure 8: *The application of the stress inversion results for Box 1 (left column) and Box 2 (right column) on Dwc1 and Dwc2 fault systems and the resulting Slip Tendency values associated with the Mohr-Coulomb stress states. The slip tendency estimate associated with each fault segment is presented as color-coded planes in both the stereoplots and their adjoining Mohr diagrams.*

5 Discussion

5.1 The Stress Regime of Earthquakes along the Western Africa Continental Margin

The regional clustering of earthquakes along and in the vicinity of preexisting tectonic lineaments (Fig. 3a) and the stress tests performed in this study (Figs. 6 - 8) show that earthquakes along the continental margin of western Africa and western Central Africa are likely associated with seismogenic reactivation of preexisting fault systems inherited from past tectonic events. These structures, consist primarily of brittle shear zones developed during the Eburnean orogeny (Proterozoic), Pan-African Orogeny (Proterozoic), and the opening of the Central and South Atlantic (Late Cretaceous). The results of stress inversion and stress tests in this study show that most of the actual fault planes would be NW-SW, NNW-SSE, N-S, NNE to NE-SW and less likely E-W trending strike-slip faults/normal faults or NW-SE and E-W trending thrust-faults in Box 1, Box 2 and Box 3 sub-regions. These faults orientations match most of the described fractures systems in the area and in the literature, particularly for Box 3 (Fig.3). In Box 1 and Box 2 sub-regions, the NW- and E-W -oriented thrust faults probably correspond to the orientation of structures within the West-Congo Belt and thrust sheets of the Oubanguides Belt respectively. Both the strike-slip faults and normal faults deform every unit in the sub-regions from Archean through the Cretaceous units. Also, based on the visited field sites with seismic events, the earthquake epicenters are generally located in the vicinity of the large strike-slip fault systems or normal fault zones. For Box 3, strike-slip faults and normal faults would likely correspond to N-S and NNE-trending strike-slip and thrust fault systems of the Dahomeyide Belt (Affaton et al., 1991; Villeneuve & Cornée, 1994) which were later reactivated either in normal faulting or strike-slip faulting.

The orientations of nodal planes used in stress inversion determination are consistent with the kinematics of some of the strike-slip, normal, and thrust fault systems with high values of slip tendency in Box 1 and Box 2 stress fields applied to these faults systems in the area (Figs. 6, 7, 8). The NNW-SSE and NNE-SSW features would play as dextral strike-slip faults and sinistral strike-slip faults under the stress regime in Box 1. This situation is satisfied in perfectly in Dso fault system of Souanké (Fig.7e) and with some faults in the Inkisi Group (Fig. 7a). For instance, in the coastal margin, the Monatélé earthquake in Cameroon was associated with a NE-SW trending strike-slip sinistral fault (Ngatchou et al., 2018). This clearly supports the kinematics of actual faults plan acting in this coastal margin. From the coastal margin to inland continent, the results show that there is a partition in stress regime within the western central African continental plate. On the coastal margin a strike-slip faulting regime with a minor compressional regime component prevails, while in the inland, the regime is more compressive with a moderate strike-slip faulting component. This explain why NW-SE to NNE-SE strike-slip faults/normal faults show the most tendency to be reactivated in the costal margin areas during the past or present-day. While for the continental interior areas, the most probable reactivated structures are NW-thrust faults/normal faults systems and less likely strike-slip faults. Delvaux et al. (2017) proposed the development of strike-slip deformation of the Inkisi Group during the opening of the south Atlantic and suggested that the event was associated with the last phase of continental break-up with sub-horizontal maximum compressive stress that is oriented N-S. The inferred stress field of the break-up phase is similar to the stress field calculated for the Box 1 stress-field in this study (Fig.6a). This would indicate that the Box 1 stress field was once acting on the cratonic interior sub-regions but is now restricted to the continental margin areas.

Overall, several studies have speculated that preexisting fractures are hosting earthquakes along the continental margins and interior of western Africa but lack details of the ambient stress field and the evidence for coseismic surface fault rupture or presence of active fault scarps (Blundell, 1976; Sykes, 1978; Bouka Biona and Sounga, 2001; Bouka Biona and Sounga, 2001; Ayele, 2002; Amponsah, 2002; Kutu, 2013; Olugboji et al., 2021). Here, with our stress analysis, we provide insight into the control of contemporary stress regimes on the occurrence of intraplate earthquakes in the region.

5.2 The Inherited Weakness of the Preexisting Fault Systems

Our stress analysis shows that the structural geometries of preexisting fault zone fracture surfaces make them favorably oriented for reactivation in the contemporary stress field. However, although fault orientation and their coefficient of friction in the Mohr-Coulomb space may determine whether a preexisting fault can reactivate, they do not determine whether faults would reactivate by stable creep or by seismic rupture. The susceptibility of faults to seismic or stable creep reactivation is determined by the frictional stability of the faulted rocks at the contemporary temperature and pressure conditions at depth in the crust (Blanpied et al., 1998; Dieterich, 1979; Ikari et al., 2011; Marone, 1998). This phenomenon is true for both active plate boundary settings (e.g., Carpenter et al., 2009) and intraplate settings (e.g., Kolawole et al., 2019).

Our field observations of the basement- and sedimentary-hosted fault systems show widespread occurrence of hydrothermal alterations along the fault zones (Fig.5). These hydrothermal alterations include calcite veins, quartz veins, palygorskite gouge fill, a mix of palygorskite and calcite, and iron stains along the fault planes. Also, we note that the fault zones commonly show post-alteration brittle reactivation of the fault zones (e.g., Figs.5b, c, d). The presence of accretion patterns in the calcite realms suggest that there were multiple episodes of hydrothermal incursion into the fault zones. Also, the presence of calcite alterations along fault zones in both the crystalline basement rocks of the West Congo Belt and overlying Inkisi Sandstone units suggest that the large strike-slip fault systems in the sandstone exposures are likely rooted directly into the basement and both structural levels have shared at least one episode of hydrothermal circulation in the past. However, more importantly, the most-common alteration minerals along the fault zones, calcite and palygorskite, are known from laboratory experiments to show frictional instability ($0 > a-b > -0.013$) at temperature and pressure conditions relevant to a seismogenic depth interval in the upper crust (Kolawole et al., 2019; Sánchez-Roa et al., 2017; Verberne et al., 2015).

Overall, the fault zones investigated in the field are generally dry in present-day. Also, asides from the Cameroon Volcanic Line and the Angolan Bié Dome, hot springs are very rare and there is no large-scale geothermal high-anomaly along the western Africa onshore continental margin areas (Macgregor, 2020; Waring et al., 1965). The occurrence of hot springs in both the Cameroon Volcanic Line and Bié Dome are understandable since both are known zones of localized mantle upwelling (Reusch et al., 2010; Walker et al., 2016). The sparseness of hot springs in the region suggests that seismic reactivation of the intraplate fault zones is not likely driven by crustal circulation of hot fluids. Therefore, considering the widespread occurrence of minerals like calcite, quartz, and palygorskite along the fault zones, we suggest that the seismic stability conditions of the faulted rocks at depth may be contributing to the susceptibility of the onshore fault zones to seismic reactivation.

5.3 Possible Origins of Stress Loading along the Western Africa Continental Margin

Again, aside from the Cameroon Volcanic Line and Bié Dome in Angola, where active mantle processes are driving magmatic activities and associated earthquakes (De Plaen et al., 2014; Tabod et al., 1992; Ubangoh et al., 1997), the origin of stress loading leading to seismogenic rupture of preexisting faults in the onshore areas of the western Africa's continental margin remains controversial and less understood (Olugboji et al., 2021). The proposed mechanisms include the reactivation of local basement fractures by far-field tectonic stresses from mantle processes along the Cameroon volcanic line, post-rift crustal relaxation along the rifted margin, landward continuation of oceanic fracture zones, and induced earthquakes triggered by groundwater extraction (Olugboji et al., 2021).

The zone of earthquake clustering along the Ghanian coastal margin, shown in Fig. 3a, is collocated with NNE-trending Quaternary faults (Akwapim, Lokossa, and Séhoué Faults) which splay northwards from the northeastern tip zone of the Chain Fracture Zone offshore, defining a Reidel horsetail-pattern geometry within the fracture zone (Burke, 1969). However, (Burke, 1969) rightfully noted that there is no evidence of continuity of fault trace further inland from this region. However, just east of the Ghana region, brittle deformation of basement massifs further inland in SW Nigeria show the pervasive presence of satellite-scale ENE-trending fracture systems (Anifowose & Kolawole, 2012) that trend parallel to the near-shore segments of the oceanic fracture zones. Likewise, in this study, onshore large-scale lineament mapping and detailed field mapping of fault systems show the presence of ENE-to-NE-trending fault systems that do not extend directly offshore, but also trend parallel to the near-shore segments of the oceanic fracture zones (Figs. 1, 3a). It was also proposed that channeling of melt along the northeastward extension of the Ascension Fracture Zone across the continent-ocean boundary and further onshore influenced the development of the Cameroon Volcanic Line (Reusch et al., 2010). However, the NE-SW oriented extensional structures would have formed parallel to the shortening axis and approximately to the maximum compressive stress (Woodcock & Schubert, 1994).

In addition to the observation of similar structural trends between oceanic fracture zones and onshore fault and fracture systems, our analysis shows that the stresses acting on the offshore oceanic fracture zones are comparable with the stresses acting along the onshore areas of the continental margin (Figs. 6a-b and 6e); and that the onshore fault systems have a high slip tendency in this contemporary stress field (Figs. 7-8). Given that the oceanic fracture zones are active intraplate faults possibly activated by far-field strain transfer from transform faults along the spreading ridges (Fig. 2a; Meghraoui et al., 2019), we propose that northeastward stress propagation into the near-shore and onshore tip zones of the oceanic fracture zones may be driving stress loading on pre-stressed fault systems onshore, leading to fault reactivation in the onshore areas.

6 Conclusions

In this study, we compute the contemporary stress field along the coastal margin of western Africa and some of the interior cratonic areas, map pre-existing fault systems in basement and sedimentary outcrops along the margin, and access the reactivation potential of the mapped structural planes. Our results show that:

- Intraplate earthquakes along the continental margin of West Africa and western Central Africa cluster along or in the vicinity of preexisting brittle shear zones and thrust faults, suggesting a potential for brittle reactivation of preexisting structures.
- The earthquakes originate under a transpressive stress regime with the maximum principal compressive stress ($\sigma 1$, parallel to SHmax) oriented NNE-SSW.
- In this contemporary stress field, the pre-existing NNE-, NNW-, and N-S -trending strike-slip faults and normal faults show a high slip tendency (60 – 100 %), suggesting a high likelihood to be reactivated. Whereas in the cratonic interior of western Central Africa, the NW- and N-S -trending thrust faults are the most probable structures to be reactivated.
- In both the basement and sedimentary cover rocks, paleo- hydrothermal alterations of the fault zones are common. Although, in present-day, the fault zones are generally dry, the

high likelihood of reactivation (based on our stress tests) and presence of fault rock frictionally unstable materials on fault planes (minerals like palygorskite and calcite) suggest that the faults may be susceptible to frictional instability and earthquake nucleation during their reactivation.

- Our stress analysis show that the regional stresses acting on offshore oceanic fracture zones are compatible with the stresses acting along the onshore areas of the continental margin; and that the onshore pre-existing strike-slip faults, which are parallel to the oceanic fracture zones, have a high slip tendency in this contemporary stress field.
- We propose that northeastward stress propagation into the near-shore and onshore tip zones of the oceanic fracture zones may be driving stress loading on pre-stressed fault systems onshore, leading to fault reactivation in the onshore areas.

Acknowledgments

The authors declare that they have no known competing financial interests or personal relationships that could have appeared to influence the work reported in this paper. This work is part of the PhD thesis of Nkodia Hardy. It is funded by Coopération Belge and ACCORDCAD, under the GEORES4DEV program, for his PhD through the support of the Royal Museum of Central Africa. We thank the reviewers for their great help to improve this manuscript. We also thank Mr. Elvis Kongota and Prof. Valentin Kanda Nkula for their administrative help in Democratic Republic of Congo.

Data Availability Statement

The earthquake data used in this study can be downloaded in the International Seismic Center (ISC), the United States Geological Survey (USGS), the Global Centroid-Moment-Tensor (CMT), and the GFZ GEOFON earthquake catalogs. The focal mechanism data and field measurements that support the analysis in this study are provided in the supplementary documents of the manuscript. The version 5.9.1 of the Win-Tensor free-access software was used to determine stress from focal mechanism and for the assessment of fault slip tendency. The software can be downloaded from http://damiendelvaux.be/Tensor/tensor-index.html (D. Delvaux, 2012).

Credit Author statement

DVMHN: Conceptualization, Methodology, Data Curation, Investigation, Writing-Original; Writing- review & editing; Visualization, Formal analysis, Project administration; **TM**: Conceptualization; Methodology, Investigation; Reviewing; **FK**: Methodology, Writing- review & editing, Visualization, Validation; **FB**: Conceptualization, Investigation, Supervision, Project administration, Funding Acquisition, Reviewing; **APRL**: Investigation; reviewing; **NCBT**: Investigation and reviewing; **DD**: Methodology, Writing- review & editing, Supervision, Investigation; Validation; Resources, Data Curation, Funding Acquisition.

References

Adepelumi, A. A., Ako, B. D., Ajayi, T. R., Olorunfemi, A. O., Awoyemi, M. O., & Falebita, D. E. (2008). Integrated geophysical mapping of the Ifewara transcurrent fault system, Nigeria. *Journal of African Earth Sciences*, *52*(4), 161–166. https://doi.org/10.1016/j.jafrearsci.2008.07.002

Affaton, P., Rahaman, M. A., Trompette, R., & Sougy, J. (1991). The Dahomeyide Orogen: tectonothermal evolution and relationships with the Volta Basin. In *The West African orogens and circum-Atlantic correlatives* (pp. 107–122). Springer.

Ajakaiye, D., Hall, D., Millar, T., Verheijen, P., Awad, M., & Ojo, S. (1986). Aeromagnetic anomalies and tectonic trends in and around the Benue Trough, Nigeria. *Nature*, *319*, 582–584. https://doi.org/10.1038/319582a0

Akame, J. M., Owona, S., Hublet, G., & Debaille, V. (2020). Archean tectonics in the sangmelima granite-greenstone terrains, Ntem Complex (NW Congo craton), southern Cameroon. *Journal of African Earth Sciences*, *168*, 103872. https://doi.org/10.1016/j.jafrearsci.2020.103872

Akame, J. M., Schulz, B., Owona, S., & Debaille, V. (2021). Monazite EPMA-CHIME dating of Sangmelima granulite and granitoid rocks in the Ntem Complex, Cameroon: Implications for Archean tectono-thermal evolution of NW Congo craton. *Journal of African Earth Sciences*, *181*, 104268. https://doi.org/10.1016/j.jafrearsci.2021.104268

Alvarez, P., & Maurin, J.-C. (1991). Evolution sédimentaire et tectonique du bassin protdrozoïque supérieur de Comba (Congo): stratigraphie séquentielle du Supergroupe Ouest-Congolien et modèle d'amortissement sur décrochements dans le contexte de la tectogènèse panafricaine, *50*, 137–171.

Ambraseys, N. N., & Adams, R. D. (1986). Seismicity of West Africa. *Seismicity of West Africa*, *4*(6), 679–702.

Amponsah, P., Leydecker, G., & Muff, R. (2012). Earthquake catalogue of Ghana for the time period 1615–2003 with special reference to the tectono-structural evolution of south-east Ghana. *Journal of African Earth Sciences*, *75*, 1–13. https://doi.org/10.1016/j.jafrearsci.2012.07.002

Amponsah, P. E. (2002). Seismic activity in relation to fault systems in southern Ghana. *Journal of African Earth Sciences*, *35*(2), 227–234. https://doi.org/10.1016/S0899-5362(02)00100-8

Angelier, J. (1975). Sur l'analyse de mesures recueillies dans des sites faillés: l'utilité d'une confrontation entre les méthodes dynamiques et cinématiques: erratum. *Comptes-Rendus de l'Académie Des Sciences*, *283*, 466.

Angelier, J. (1989). From orientation to magnitudes in paleostress determinations using fault slip data. *Journal of structural geology*, *11*(1/2), 37–50.

Angelier, J., & Mechler, P. (1977). Sur une methode graphique de recherche des contraintes principales egalement utilisables en tectonique et en seismologie : la methode des diedres droits. *Bulletin de La Société Géologique de France*, *S7-XIX*(6), 1309–1318. https://doi.org/10.2113/gssgfbull.S7-XIX.6.1309

Anifowose, A. Y. B., & Kolawole, F. (2012). Emplacement Tectonics of Idanre Batholith, West Africa. *Comunicações Geológicas*, *99*(2).

Antobreh, A. A., Faleide, J. I., Tsikalas, F., & Planke, S. (2009). Rift–shear architecture and tectonic development of the Ghana margin deduced from multichannel seismic reflection and potential field data. *Marine and Petroleum Geology*, *26*(3), 345–368. https://doi.org/10.1016/j.marpetgeo.2008.04.005

Assumpção, M. (1998). Seismicity and stresses in the Brazilian passive margin. *Bulletin of the Seismological Society of America*, *88*(1), 160–169.

Awoyemi, M., & Onyedim, G. (2004). Relationship between air photo lineament and fracture patterns of Ilesha, southwestern Nigeria. *African Geoscience Review*, *11*(1), 81–90.

Awoyemi, M. O., Hammed, O. S., Falade, S. C., Arogundade, A. B., Ajama, O. D., Iwalehin, P. O., & Olurin, O. T. (2017). Geophysical investigation of the possible extension of Ifewara fault zone beyond Ilesa area, southwestern Nigeria. *Arabian Journal of Geosciences*, *10*(2), 27. https://doi.org/10.1007/s12517-016-2813-z

Batumike, M. J., Kampunzu, A. B., & Cailteux, J. H. (2006). Petrology and geochemistry of the Neoproterozoic Nguba and Kundelungu Groups, Katangan Supergroup, southeast Congo: implications for provenance, paleoweathering and geotectonic setting. *Journal of African Earth Sciences*, *44*(1), 97–115.

Benkhelil, J. (1989). The origin and evolution of the Cretaceous Benue Trough (Nigeria). *Journal of African Earth Sciences (and the Middle East)*, *8*(2–4), 251–282.

Blanpied, M. L., Tullis, T. E., & Weeks, J. D. (1998). Effects of slip, slip rate, and shear heating on the friction of granite. *Journal of Geophysical Research: Solid Earth*, *103*(B1), 489–511. https://doi.org/10.1029/97JB02480

Blundell, D. J. (1976). Active faults in West Africa. *Earth and Planetary Science Letters*, *31*(2), 287–290. https://doi.org/10.1016/0012-821X(76)90221-1

Boudzoumou, F., & Trompette, R. (1988). La chaine panafricaine ouest-congolienne au Congo (Afrique equatoriale); un socle polycyclique charrie sur un domaine subautochtone forme par l'aulacogene du Mayombe et le bassin de l'Ouest-Congo. *Bulletin de La Société Géologique de France*, *4*(6), 889–896.

Bouenitela, T. T. V. (2019). *LE DOMAINE PALEOPROTEROZOIQUE (EBURNEEN) DE LA CHAINE DU MAYOMBE (CONGO-BRAZZAVILLE) : origine et évolution tectono-métamorphique*. Université de Rennes 1, Rennes.

Bouka Biona, C., & Sounga, J.-D. (2001). Corrélation entre la localisation des foyers des séismes et les zones de délimination des horsts et des grabens su soubassement de la Cuvette Congolaise (Afrique Centrale). *Annales Université Brazzaville*, *2*(1), 125–139.

Burbank, D. W., & Anderson, R. S. (2011). *Tectonic Geomorphology*. John Wiley & Sons.

Burke, K. (1969). Seismic Areas of the Guinea Coast where Atlantic Fracture Zones reach Africa. *Nature*, *222*(5194), 655–657. https://doi.org/10.1038/222655b0

Calais, E., Camelbeeck, T., Stein, S., Liu, M., & Craig, T. J. (2016). A new paradigm for large earthquakes in stable continental plate interiors. *Geophysical Research Letters*, *43*(20), 10,621-10,637. https://doi.org/10.1002/2016GL070815

Carpenter, B. M., Marone, C., & Saffer, D. M. (2009). Frictional behavior of materials in the 3D SAFOD volume. *Geophysical Research Letters*, *36*(5). https://doi.org/10.1029/2008GL036660

De Carvalho, H., Tassinari, C., Alves, P. H., Guimarães, F., & Simões, M. C. (2000). Geochronological review of the Precambrian in western Angola: links with Brazil. *Journal of African Earth Sciences*, *31*(2), 383–402. https://doi.org/10.1016/S0899-5362(00)00095-6

De Long, S. E., Dewey, J. F., & Fox, P. J. (1977). Displacement history of oceanic fracture zones. *Geology*, *5*(4), 199–202. https://doi.org/10.1130/0091-7613(1977)5<199:DHOOFZ>2.0.CO;2

De Plaen, R. S. M., Bastow, I. D., Chambers, E. L., Keir, D., Gallacher, R. J., & Keane, J. (2014). The development of magmatism along the Cameroon Volcanic Line: Evidence from seismicity and seismic anisotropy. *Journal of Geophysical Research: Solid Earth*, *119*(5), 4233–4252. https://doi.org/10.1002/2013JB010583

Delteil, J.-R., Valery, P., Montadert, L., Fondeur, C., Patriat, P., & Mascle, J. (1974). Continental Margin in the Northern Part of the Gulf of Guinea. In C. A. Burk & C. L. Drake (Eds.), *The Geology of Continental Margins* (pp. 297–311). Berlin, Heidelberg: Springer. https://doi.org/10.1007/978-3-662-01141-6_22

Delvaux, D. (2012). Release of program Win-Tensor 4.0 for tectonic stress inversion: statistical expression of stress parameters. In *Geophysical research abstracts* (Vol. 14). EGU General Assembly Vienna.

Delvaux, Damien, & Bath. (2010). African stress pattern from formal inversion of focal mechanism data. *Tectonophysics*, *482*, 105–128.

Delvaux, Damien, Everaerts, M., Kongota Isasi, E., & Ganza Bamulezi, G. (2016). Intraplate compressional deformation in West-Congo and the Congo basin: related to ridge-puch from the South Atlantic spreading ridge? In *EGU General Assembly Conference Abstracts* (Vol. 18).

Delvaux, Damien, Ganza, G., Kongota, E., Fukiabantu, G., Mbokola, D., Boudzoumou, F., et al. (2017). The" fault of the Pool" along the Congo River between Kinshasa and Brazzaville, R (D) Congo is no more a myth: Paleostress from small-scale brittle structures. In *EGU General Assembly Conference Abstracts* (Vol. 19, p. 15143).

Delvaux, Damien, Maddaloni, F., Tesauro, M., & Braitenberg, C. (2021). The Congo Basin: Stratigraphy and subsurface structure defined by regional seismic reflection, refraction and well data. *Global and Planetary Change*, *198*, 103407. https://doi.org/10.1016/j.gloplacha.2020.103407

Dieterich, J. H. (1979). Modeling of rock friction: 1. Experimental results and constitutive equations. *Journal of Geophysical Research: Solid Earth*, *84*(B5), 2161–2168. https://doi.org/10.1029/JB084iB05p02161

Fail, J. P., Montadert, L., Delteil, J. R., Valery, P., Patriat, Ph., & Schlich, R. (1970). Prolongation des zones de fractures de l'ocean atlantique dans le golfe de guinee. *Earth and Planetary Science Letters*, *7*(5), 413–419. https://doi.org/10.1016/0012-821X(70)90083-X

Fullgraf, T., Callec, Y., Thiéblemont, D., Gloaguen, E., Charles, N., Métour, J., et al. (2015). *Notice explicative de la carte géologique de la République du Congo à 1/200 000, Feuille Dolisie.* (F). République du Congo: Editions BRGM.

Gatsé Ebotehouna, C., Xie, Y., Adomako-Ansah, K., Gourcerol, B., & Qu, Y. (2021). Depositional Environment and Genesis of the Nabeba Banded Iron Formation (BIF) in the Ivindo Basement Complex, Republic of the Congo: Perspective from Whole-Rock and Magnetite Geochemistry. *Minerals*, *11*(6), 579. https://doi.org/10.3390/min11060579

GEBCO Bathymetric Compilation Group 2021. (2021). The GEBCO_2021 Grid - a continuous terrain model of the global oceans and land. *NERC EDS British Oceanographic Data Centre NOC*. https://doi.org/doi:10.5285/c6612cbe-50b3-0cff-e053-6c86abc09f8f

Gerya, T. (2012). Origin and models of oceanic transform faults. *Tectonophysics*, *522–523*, 34–54. https://doi.org/10.1016/j.tecto.2011.07.006

Gorini, M. A., & Bryan, G. (1976). The tectonic fabric of the equatorial Atlantic and adjoining continental margins: Gulf of Guinea to the northeastern Brazil. (Vol. 48, pp. 101–119). Presented at the An. Acad. Brasil. Cienc., Sao Paulo.

Grigoli, F., Cesca, S., Priolo, E., Rinaldi, A. P., Clinton, J. F., Stabile, T. A., et al. (2017). Current challenges in monitoring, discrimination, and management of induced seismicity related to underground industrial activities: A European perspective. *Reviews of Geophysics*, *55*(2), 310–340.

Guiraud, M., Buta-Neto, A., & Quesne, D. (2010). Segmentation and differential post-rift uplift at the Angola margin as recorded by the transform-rifted Benguela and oblique-to-orthogonal-rifted Kwanza basins. *Marine and Petroleum Geology*, *27*(5), 1040–1068. https://doi.org/10.1016/j.marpetgeo.2010.01.017

Gupta, H. K., Rastogi, B. K., Mohan, I., Rao, C. V. R. K., Sarma, S. V. S., & Rao, R. U. M. (1998). An investigation into the Latur earthquake of September 29, 1993 in southern India. *Tectonophysics*, *287*(1), 299–318. https://doi.org/10.1016/S0040-1951(98)80075-9

Heezen, B. C., Bunce, E. T., Hersey, J. B., & Tharp, M. (1964). Chain and romanche fracture zones. *Deep Sea Research and Oceanographic Abstracts*, *11*(1), 11–33. https://doi.org/10.1016/0011-7471(64)91079-4

Heezen, B. C., Tharp, M., Blackett, P. M. S., Bullard, E., & Runcorn, S. K. (1965). Tectonic fabric of the Atlantic and Indian oceans and continental drift. *Philosophical Transactions of the Royal Society of London. Series A, Mathematical and Physical Sciences*, *258*(1088), 90–106. https://doi.org/10.1098/rsta.1965.0024

Hensen, C., Duarte, J. C., Vannucchi, P., Mazzini, A., Lever, M. A., Terrinha, P., et al. (2019). Marine Transform Faults and Fracture Zones: A Joint Perspective Integrating Seismicity, Fluid Flow and Life. *Frontiers in Earth Science*, *7*, 39. https://doi.org/10.3389/feart.2019.00039

Holford, S. P., Hillis, R. R., Hand, M., & Sandiford, M. (2011). Thermal weakening localizes intraplate deformation along the southern Australian continental margin. *Earth and Planetary Science Letters*, *305*(1), 207–214. https://doi.org/10.1016/j.epsl.2011.02.056

Hossié, G. (1980). *Contribution à l'étude structurale de la chaîne ouest-congolienne(pan-africaine) dans le Mayombe congolais.* (Thesis). University of Montpellier, Montpellier.

Ikari, M. J., Marone, C., & Saffer, D. M. (2011). On the relation between fault strength and frictional stability. *Geology*, *39*(1), 83–86. https://doi.org/10.1130/G31416.1

Jelsma, H. A., McCourt, S., Perritt, S. H., & Armstrong, R. A. (2018). The Geology and Evolution of the Angolan Shield, Congo Craton. In S. Siegesmund, M. A. S. Basei, P. Oyhantçabal, & S. Oriolo (Eds.), *Geology of Southwest Gondwana* (pp. 217–239). Cham: Springer International Publishing. https://doi.org/10.1007/978-3-319-68920-3_9

Junner, N. R., & Bates, D. A. (1941). *The accra earthquake of 22nd June, 1939*. FJ Miller.

Kadima, E., Delvaux, D., Sebagenzi, S. N., Tack, L., & Kabeya, S. M. (2011). Structure and geological history of the Congo Basin: an integrated interpretation of gravity, magnetic and reflection seismic data. *Basin Research*, *23*(5), 499–527.

Kadiri, A. U., & Kijko, A. (2021). Seismicity and seismic hazard assessment in West Africa. *Journal of African Earth Sciences*, *183*, 104305. https://doi.org/10.1016/j.jafrearsci.2021.104305

Keranen, K. M., & Weingarten, M. (2018). Induced Seismicity. *Annual Review of Earth and Planetary Sciences*, *46*(1), 149–174. https://doi.org/10.1146/annurev-earth-082517-010054

Kessi, C. (1992). *Le socle Archéen et les formations ferrifères du Chaillu au Congo* (Thèse Doctorat). Université de Rennes 1, Rennes.

Kolawole, F., Johnston, C. S., Morgan, C. B., Chang, J. C., Marfurt, K. J., Lockner, D. A., et al. (2019). The susceptibility of Oklahoma's basement to seismic reactivation. *Nature Geoscience*, *12*(10), 839–844. https://doi.org/10.1038/s41561-019-0440-5

Kolawole, Folarin, Atekwana, E. A., Malloy, S., Stamps, D. S., Grandin, R., Abdelsalam, M. G., et al. (2017). Aeromagnetic, gravity, and Differential Interferometric Synthetic Aperture Radar analyses reveal the causative fault of the 3 April 2017 Mw 6.5 Moiyabana, Botswana, earthquake. *Geophysical Research Letters*, *44*(17), 8837–8846.

Krenkel, E. (1923). Die Seismizität Afrikas. *Zentralbl. Mineral. Geol. Palaeontol*, *6*, 173–183.

Kutu, J. M. (2013). Seismic and Tectonic Correspondence of Major Earthquake Regions in Southern Ghana with Mid-Atlantic Transform-Fracture Zones. *International Journal of Geosciences*, *2013*. https://doi.org/10.4236/ijg.2013.410128

Lay, T. (2019). Chapter 4 - Reactivation of Oceanic Fracture Zones in Large Intraplate Earthquakes? In J. C. Duarte (Ed.), *Transform Plate Boundaries and Fracture Zones* (pp. 89–104). Elsevier. https://doi.org/10.1016/B978-0-12-812064-4.00004-9

Levandowski, W., Zellman, M., & Briggs, R. (2017). Gravitational body forces focus North American intraplate earthquakes. *Nature Communications*, *8*(1), 1–9.

Lisle, R. J., & Srivastava, D. C. (2004). Test of the frictional reactivation theory for faults and validity of fault-slip analysis. *Geology*, *32*(7), 569. https://doi.org/10.1130/G20408.1

Loemba, A. P. A., Nkodia, H. M. D.-V., Bazebizonza Tchiguina, N. C., Miyouna, T., & Boudzoumou, F. (2022). Tectonic and structural evolution of major shear zone in the Ntem-Chaillu Block, in the Ivindo region, in Republic of Congo (p. 53). Presented at the Tectonic Studies Group 2022, Online.

Lund Snee, J.-E., & Zoback, M. D. (2020). Multiscale variations of the crustal stress field throughout North America. *Nature Communications*, *11*(1), 1951. https://doi.org/10.1038/s41467-020-15841-5

Macgregor, D. S. (2020). Regional variations in geothermal gradient and heat flow across the African plate. *Journal of African Earth Sciences*, *171*, 103950. https://doi.org/10.1016/j.jafrearsci.2020.103950

Marone, C. (1998). Laboratory-Derived Friction Laws and Their Application to Seismic Faulting. *Annual Review of Earth and Planetary Sciences*, *26*(1), 643–696. https://doi.org/10.1146/annurev.earth.26.1.643

Mascle, J., & Sibuet, J.-C. (1974). New pole for early opening of South Atlantic. *Nature*, *252*(5483), 464–465.

Mbéri Kongo, M. T. G. (2018). *Tectonique de la série des plateaux Batékés dans la zone de Inoni et d'Ekoti ya MonSeigneur, République du Congo* (Master thesis). Marien Ngouabi, Brazzaville. https://doi.org/10.13140/RG.2.2.14583.34729

McCaffrey, R. (2008). Global frequency of magnitude 9 earthquakes. *Geology*, *36*(3), 263–266. https://doi.org/10.1130/G24402A.1

Meghraoui, M., Amponsah, P., Bernard, P., & Ateba, B. (2019). Active transform faults in the Gulf of Guinea: insights from geophysical data and implications for seismic hazard assessment. *Canadian Journal of Earth Sciences*, *56*(12), 1398–1408. https://doi.org/10.1139/cjes-2018-0321

Milesi, J. P., Frizon de Lamotte, D., de Kock, G., & Toteu, F. (2010). Tectonic map of Africa (2nd edition).

Miranda, T., S., Neves, S., P., Celstino, M.-A., L., & Roberts, N., M. W. (2020). Structural evolution of the Cruzeiro do Nordeste shear zone (NE Brazil): Brasiliano-Pan-African- ductile-to-brittle transition and Cretaceous brittle reactivation. *Journal of Structural Geology*, *141*, 1–17.

Miyouna, T., Dieu-Veill Nkodia, H. M., Essouli, O. F., Dabo, M., Boudzoumou, F., & Delvaux, D. (2018). Strike-slip deformation in the Inkisi Formation, Brazzaville, Republic of Congo. *Cogent Geoscience*, *4*(1), 1542762.

Morris, A., Ferrill, D. A., & Henderson, D. B. (1996). Slip-tendency analysis and fault reactivation. *Geology*, *24*(3), 275–278. https://doi.org/10.1130/0091-7613(1996)024<0275:STAAFR>2.3.CO;2

Moulin, M., Aslanian, D., & Unternehr, P. (2010). A new starting point for the South and Equatorial Atlantic Ocean. *Earth-Science Reviews*, *98*(1–2), 1–37.

Musson, R. M. W. (1992). The seismicity of West and Central Africa. In S. J. Freeth, C. O. Ofoegbu, & K. M. Onuoha (Eds.), *Natural Hazards in West and Central Africa* (pp. 7–11). Wiesbaden: Vieweg+Teubner Verlag. https://doi.org/10.1007/978-3-663-05239-5_2

Ngako, V., Affaton, P., Nnange, J. M., & Njanko, T. (2003). Pan-African tectonic evolution in central and southern Cameroon: transpression and transtension during sinistral shear movements. *Journal of African Earth Sciences*, *36*(3), 207–214.

Ngako, Vincent, Jegouzo, P., & Nzenti, J.-P. (1991). Le cisaillement centre camerounais. Rôle structural et géodynamique dans l'orogenèse panafricaine. *Le Cisaillement Centre Camerounais. Rôle Structural et Géodynamique Dans l'orogenèse Panafricaine*, *313*(4), 457–463.

Ngatchou, H. E., Nguiya, S., Owona Angue, M., Mouzong, P. M., & Tokam, A. P. (2018). Source characterization and tectonic implications of the M4.6 Monatélé (Cameroon) earthquake of 19 March 2005. *Geological Society of South Africa*.

Njonfang, E., Ngako, V., Moreau, C., Affaton, P., & Diot, H. (2008). Restraining bends in high temperature shear zones: the "Central Cameroon Shear Zone", Central Africa. *Journal of African Earth Sciences*, *52*(1–2), 9–20.

Nkodia, H. M. D.-V., Miyouna, T., Delvaux, D., & Boudzoumou, F. (2020). Flower structures in sandstones of the Paleozoic Inkisi Group (Brazzaville, Republic of Congo): evidence for two major strike-slip fault systems and geodynamic implications. *South African Journal of Geology*, *123*(4), 531–550. https://doi.org/10.25131/sajg.123.0038

Nkodia, Hardy Medry Dieu-Veill, Boudzoumou, F., Miyouna, T., Ibarra-Gnianga, A., & Delvaux, D. (2021). A progressive episode of deformation in the foreland of the WestCongo Belt: From folding to brittle shearing, in Republic of Congo (p. 1). Presented at the European Gesociences Union, online.

Nwankwoala, H., & Orji, O. (2018). An Overview of Earthquakes and Tremors in Nigeria: Occurrences, Distributions and Implications for Monitoring. *International Journal of Geology and Earth Sciences*, *4*, 56. https://doi.org/10.32937/IJGES.4.4.2018.56-76

Ofoegbu, C. O. (1985). A review of the geology of the Benue Trough, Nigeria. *Journal of African Earth Sciences (1983)*, *3*(3), 283–291. https://doi.org/10.1016/0899-5362(85)90001-6

Oha, I. A., Okonkwo, I. A., & Dada, S. S. (2020). Wrench tectonism and intracontinental basin sedimentation: a case study of the moku sub-basin, upper benue trough, Nigeria. *J. Geogr. Geol.*, *12*(1), 65–75.

Okal, E. A., & Stewart, L. M. (1982). Slow earthquakes along oceanic fracture zones: evidence for asthenospheric flow away from hotspots? *Earth and Planetary Science Letters*, *57*(1), 75–87. https://doi.org/10.1016/0012-821X(82)90174-1

Oladejo, O. P., Adagunodo, T. A., Sunmonu, L. A., Adabanija, M. A., Enemuwe, C. A., & Isibor, P. O. (2020). Aeromagnetic mapping of fault architecture along Lagos–Ore axis, southwestern Nigeria. *Open Geosciences*, *12*(1), 376–389. https://doi.org/10.1515/geo-2020-0100

Olugboji, T. M., Shirzaei, M., Lu, Y., Adepelumi, A. A., & Kolawole, F. (2021). On the Origin of Orphan Tremors & Intraplate Seismicity in Western Africa. *Earth and Space Science Open Archive ESSOAr*.

Reusch, A. M., Nyblade, A. A., Wiens, D. A., Shore, P. J., Ateba, B., Tabod, C. T., & Nnange, J. M. (2010). Upper mantle structure beneath Cameroon from body wave tomography and the origin of the Cameroon Volcanic Line. *Geochemistry, Geophysics, Geosystems*, *11*(10). https://doi.org/10.1029/2010GC003200

Sánchez-Roa, C., Faulkner, D. R., Boulton, C., Jimenez-Millan, J., & Nieto, F. (2017). How phyllosilicate mineral structure affects fault strength in Mg-rich fault systems. *Geophysical Research Letters*, *44*(11), 5457–5467. https://doi.org/10.1002/2017GL073055

Sbar, M. L., & Sykes, L. R. (1973). Contemporary Compressive Stress and Seismicity in Eastern North America: An Example of Intra-Plate Tectonics. *GSA Bulletin*, *84*(6), 1861–1882. https://doi.org/10.1130/0016-7606(1973)84<1861:CCSASI>2.0.CO;2

Suleiman, A. S., Doser, D. I., & Yarwood, D. R. (1993). Source parameters of earthquakes along the coastal margin of West Africa and comparisons with earthquakes in other coastal margin settings. *Tectonophysics*, *222*(1), 79–91. https://doi.org/10.1016/0040-1951(93)90191-L

Sykes, L. R. (1978). Intraplate seismicity, reactivation of preexisting zones of weakness, alkaline magmatism, and other tectonism postdating continental fragmentation. *Reviews of Geophysics*, *16*(4), 621–688. https://doi.org/10.1029/RG016i004p00621

Tabod, C. T., Fairhead, J. D., Stuart, G. W., Ateba, B., & Ntepe, N. (1992). Seismicity of the Cameroon Volcanic Line, 1982–1990. *Tectonophysics*, *212*(3), 303–320. https://doi.org/10.1016/0040-1951(92)90297-J

Talwani, P. (2014). Intraplate earthquakes.

Tchameni, R., Mezger, K., Nsifa, N. E., & Pouclet, A. (2000). Neoarchæan crustal evolution in the Congo Craton: evidence from K rich granitoids of the Ntem Complex, southern Cameroon. *Journal of African Earth Sciences*, *30*(1), 133–147. https://doi.org/10.1016/S0899-5362(00)00012-9

Thiéblemont, D., Castaing, C., Billa, M., Bouton, P., & Préat, A. (2009). Notice explicative de la carte géologique et des ressources minérales de la République Gabonaise à 1/1000000. *Programme Sysmin*, *8*, 384.

Turnbull, R. E., Allibone, A. H., Matheys, F., Fanning, C. M., Kasereka, E., Kabete, J., et al. (2021). Geology and geochronology of the Archean plutonic rocks in the northeast Democratic Republic of Congo. *Precambrian Research*, *358*, in–press.

Tuttle, M. P., Schweig, E. S., Sims, J. D., Lafferty, R. H., Wolf, L. W., & Haynes, M. L. (2002). The Earthquake Potential of the New Madrid Seismic Zone. *Bulletin of the Seismological Society of America*, *92*(6), 2080–2089. https://doi.org/10.1785/0120010227

Ubangoh, R. U., Ateba, B., Ayonghe, S. N., & Ekodeck, G. E. (1997). Earthquake swarms of Mt Cameroon, West Africa. *Journal of African Earth Sciences*, *24*(4), 413–424. https://doi.org/10.1016/S0899-5362(97)00072-9

Verberne, B. A., Niemeijer, A. R., De Bresser, J. H. P., & Spiers, C. J. (2015). Mechanical behavior and microstructure of simulated calcite fault gouge sheared at 20–600°C: Implications for natural faults in limestones. *Journal of Geophysical Research: Solid Earth*, *120*(12), 8169–8196. https://doi.org/10.1002/2015JB012292

Villeneuve, M., & Cornée, J. J. (1994). Structure, evolution and palaeogeography of the West African craton and bordering belts during the Neoproterozoic. *Precambrian Research*, *69*(1), 307–326. https://doi.org/10.1016/0301-9268(94)90094-9

Walker, R. T., Telfer, M., Kahle, R. L., Dee, M. W., Kahle, B., Schwenninger, J.-L., et al. (2016). Rapid mantle-driven uplift along the Angolan margin in the late Quaternary. *Nature Geoscience*, *9*(12), 909–914. https://doi.org/10.1038/ngeo2835

Waring, G. A., Blankenship, R. R., & Bentall, R. (1965). *Thermal Springs of the United States and Other Countries: A Summary*. U.S. Government Printing Office.

Wiens, D. A., & Stein, S. (1983). Age dependence of oceanic intraplate seismicity and implications for lithospheric evolution. *Journal of Geophysical Research: Solid Earth*, *88*(B8), 6455–6468.

Wiens, D. A., & Stein, S. (1985). Implications of oceanic intraplate seismicity for plate stresses, driving forces and rheology. *Tectonophysics*, *116*(1–2), 143–162.

Wilson, J. T. (1965). A new class of faults and their bearing on continental drift. *Nature*, *207*(4995), 343–347.

Woodcock, N. H., & Schubert, C. (1994). Continental strike-slip tectonics. *Continental Deformation*, 251–263.

Zoback, M. L. (1992). Stress field constraints on intraplate seismicity in eastern North America. *Journal of Geophysical Research: Solid Earth*, *97*(B8), 11761–11782. https://doi.org/10.1029/92JB00221

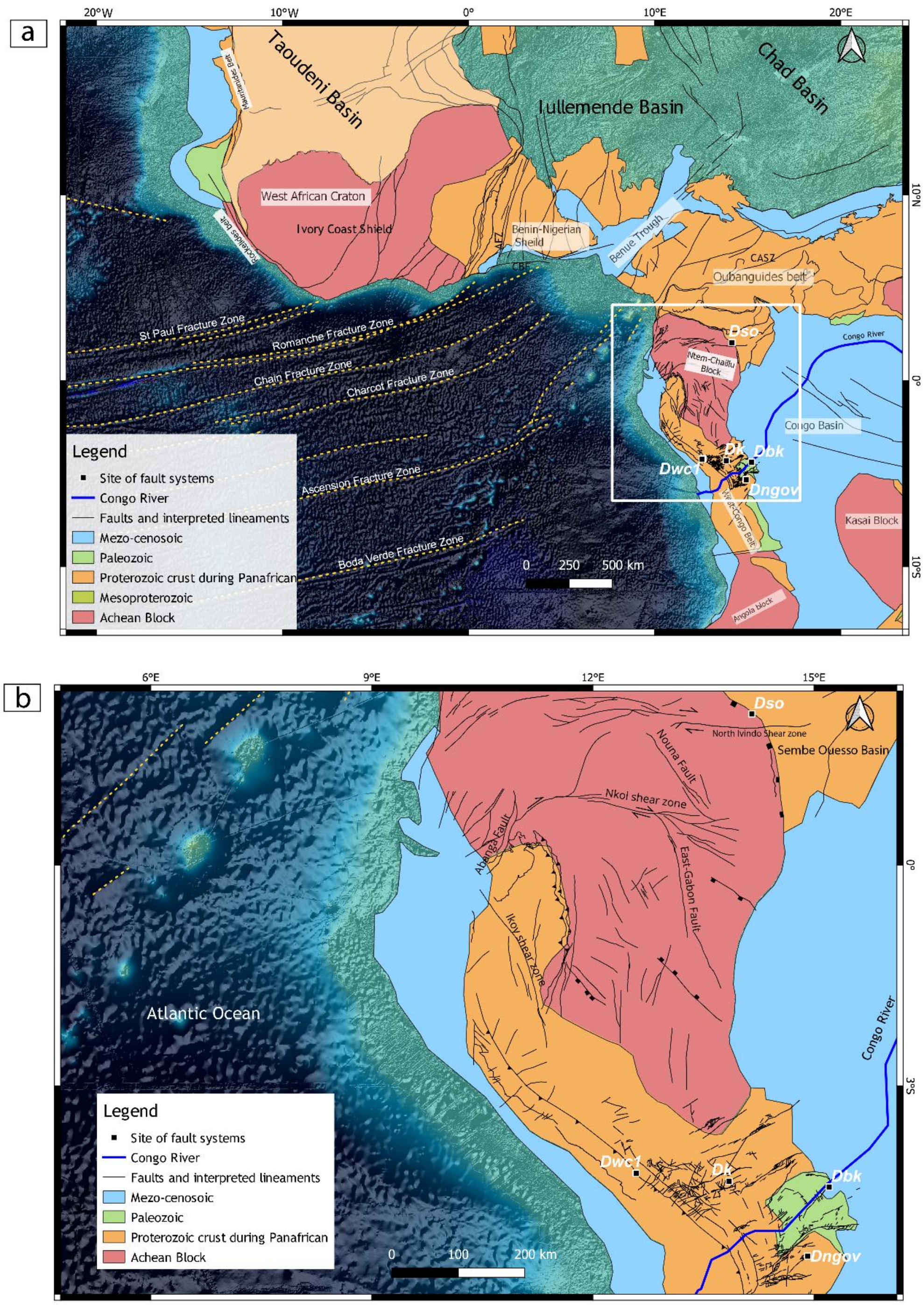

Figure 1: *Map of the bedrock geology of the Nubian Plate showing major litho-tectonic subdivisions of the crust. Dwc1, Dk, Dbk, Dngov, Dso represent field sites where structural measurements of fault systems were collected. Dwc1 represent the study site of a thrust fault system in western Congo. Dwc2 is a combination of strike-slip faults in Dk and Dngov which represent field sites in Kolas Quarry, Republic of Congo, and Ngovo Cave, Democratic Republic of Congo respectively. Dbk represents the field study sites of fault systems in Brazzaville and Kinshasa*

areas. AFZ: Akwapim Fault Zone, BFZ: Bouandary Fault Zone, CASZ: Central African shear zone.

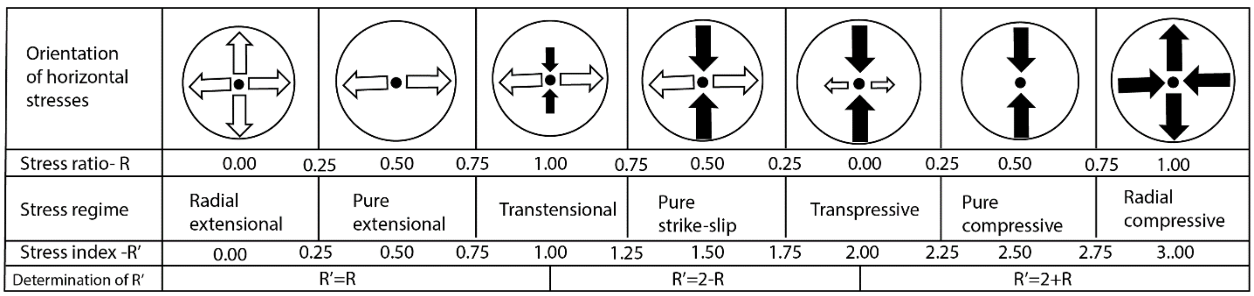

***Figure 2:** Standard values of the stress index R' with respect to the various tectonic stress regimes (modified from Delvaux et al., 2017).*

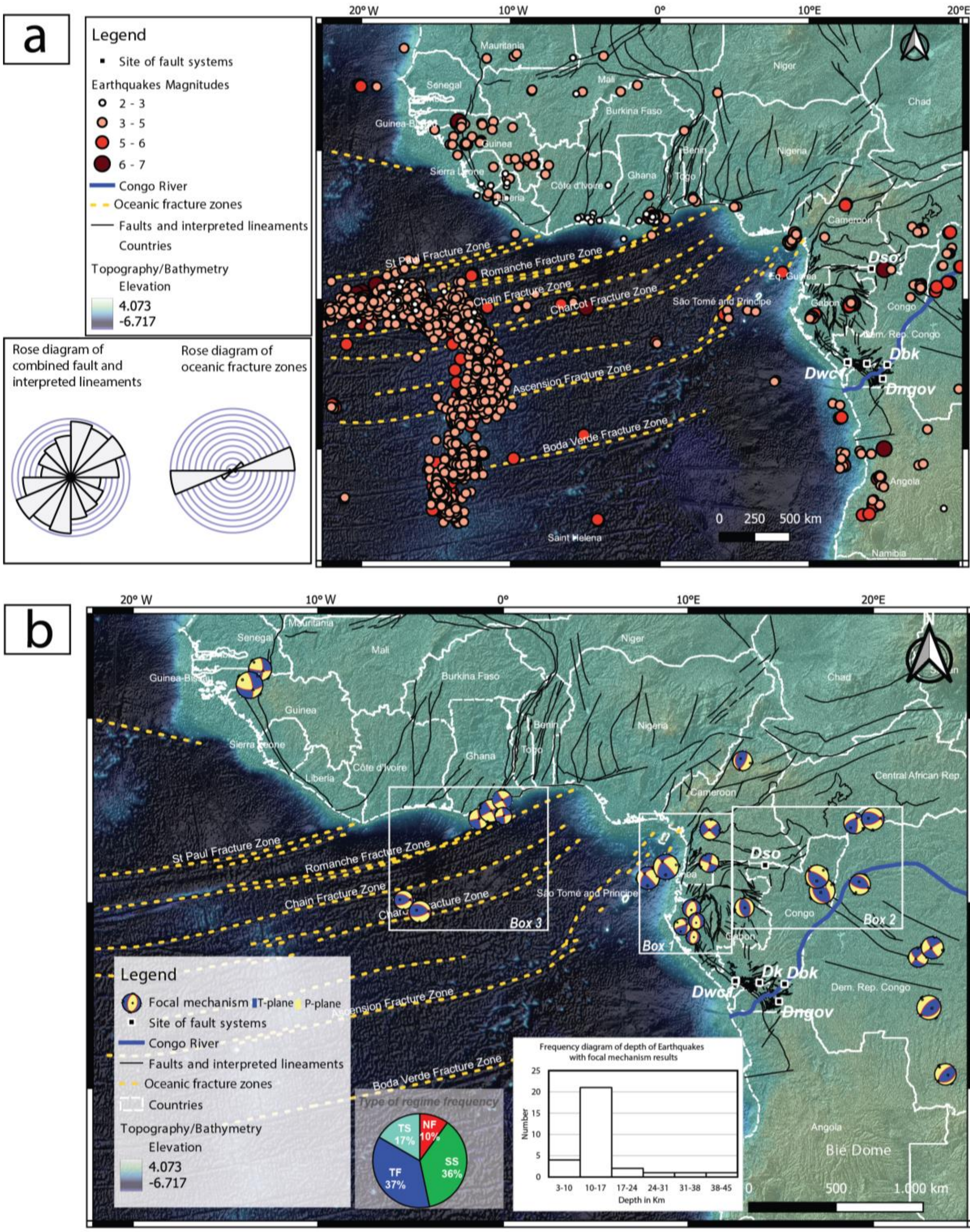

Figure 3: *(a) Map of the distribution of earthquakes in the Western African passive margin. AFZ, CASZ are the Akwapim Fault zone, the Central Africa shear zone. (b) Focal mechanisms solution for earthquakes in the western part of the Nubia Plate, obtained from several literature review, Global CMT moment tensor, and GFZ GEOFON earthquake catalogs. The boxes show the area where conducted stress inversion on focal mechanism results. The pie-chart show the frequency*

distribution of the different tectonic regime acting on the area. TS: trenstensional regime; NF: normal faulting regime; SS: strike-slip faulting regime; TF: thrust faulting regime.

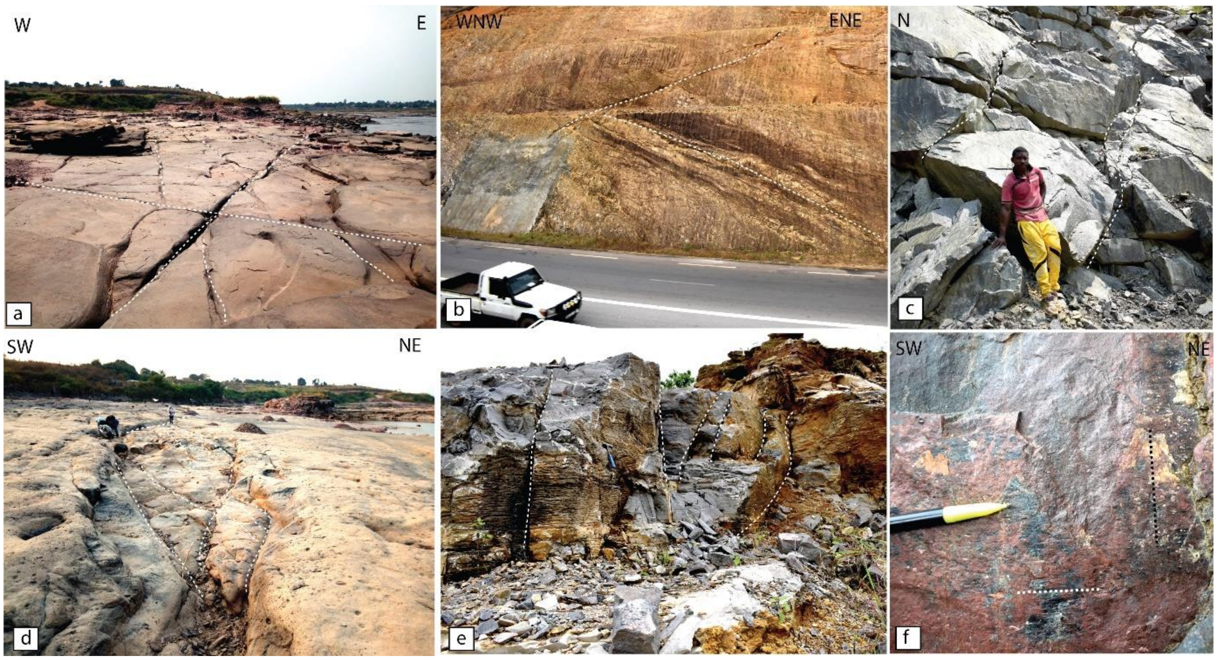

Figure 4: *Field observations of faults systems. (a & d) Fault systems in outcrops of the Inkisi Group (Dbk), showing fracture patterns (highlighted in white dashed line in 3a), and a fault zone showing segmented faults in a duplex zone (in 3d), at the Kombé quarry, located near the Congo River, Brazzaville. (b & e) Faults systems (Dwc1 & Dk) in the West-Congo Belt showing successively thrust and back-thrust affecting schists and quarzites, in Dolisie along the RN1 primary road, and strike-slip fault planes in Kolas quarry near Loutété region. (c & f) Faults systems (Dso) in Souanké showing high-angle planes of strike-slip faults in the area (in 3c) and, a NE-trending plane that shows horizontal striae that is over-printed by vertical striae associated with calcite fibers, indicating a later normal faulting reactivation of the strike-slip faults. The dashed lines in Fig. 3f represent the directions of striae.*

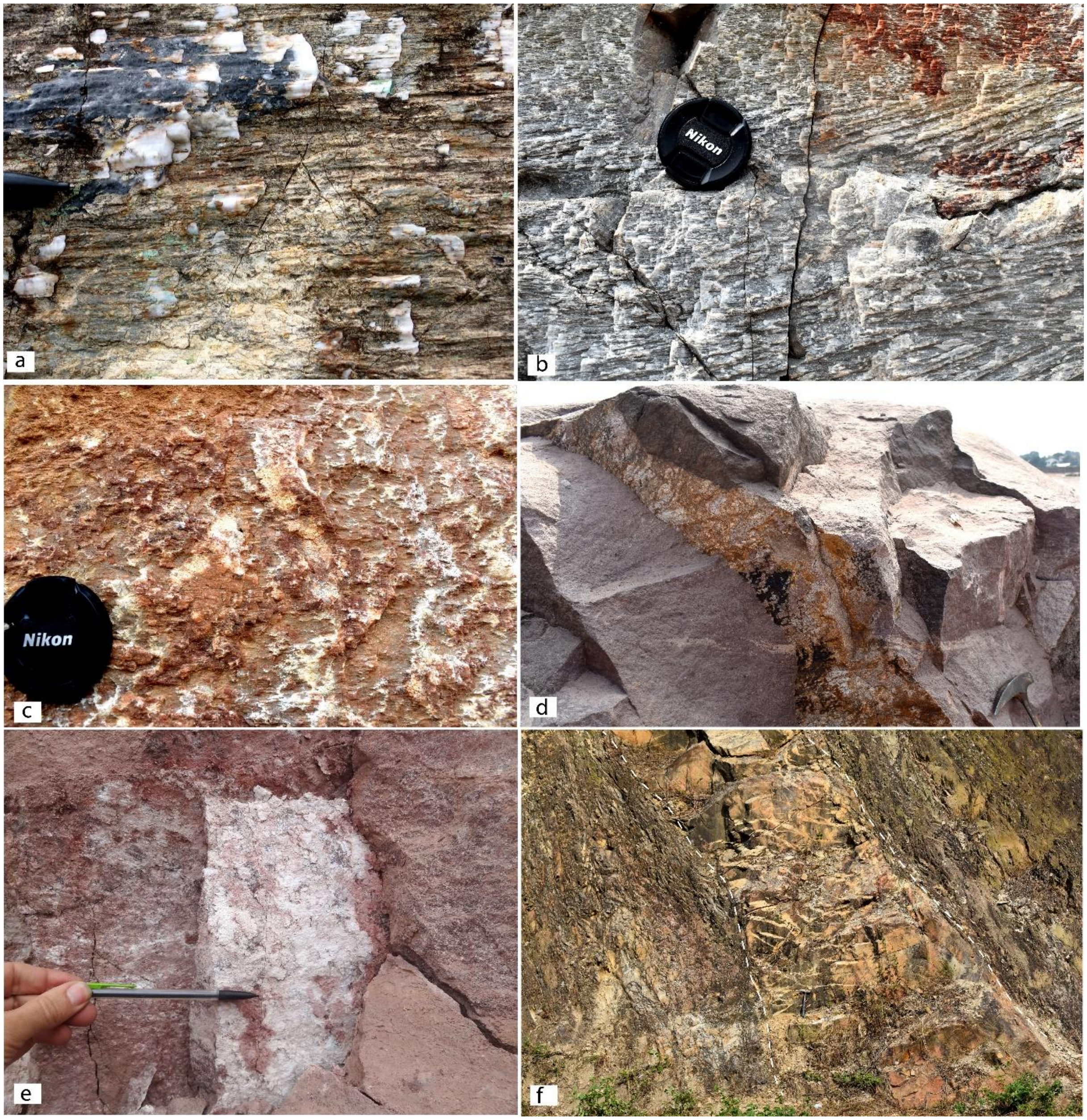

Figure 5: *Geochemical alterations along mineralized fault surfaces. (a) Accretion calcite steps along NW-SE strike-slip faults in carbonates rocks of the West Congo Belt, DRC. (b - c) Carbonate-hosted fault surfaces covered by accretion calcite steps and iron staining. Note that the carbonate rock in Figure 5b has penetrative cross-bedding structures that should not be confused with slickenlines. (d) Fault surface in Inkisi sandstones associated with iron alteration realm. (e) Slickensided palygorskite along a fault in Dbk fault system. (f) Deformed doleritic intrusion along a high-angle thrust-fault (230/40) injected with quartz veins in the Dwc1 fault system.*

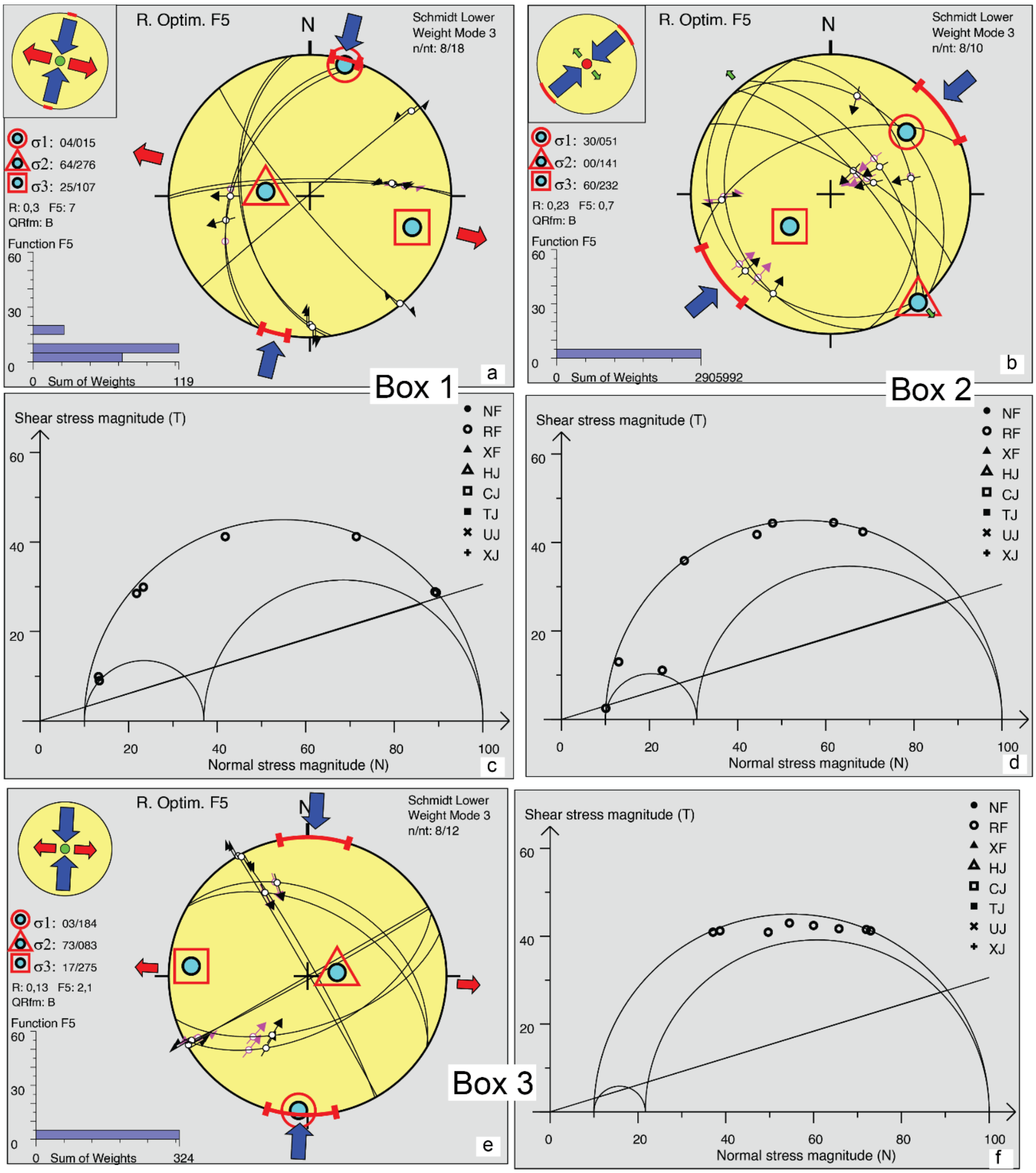

Figure 6: *Results of stress tensors from the inversion of earthquake focal mechanism solution along the western Africa continental margin, offshore and onshore Gulf of Guinea represented by sub-regional boxes (see Fig, 3b).*

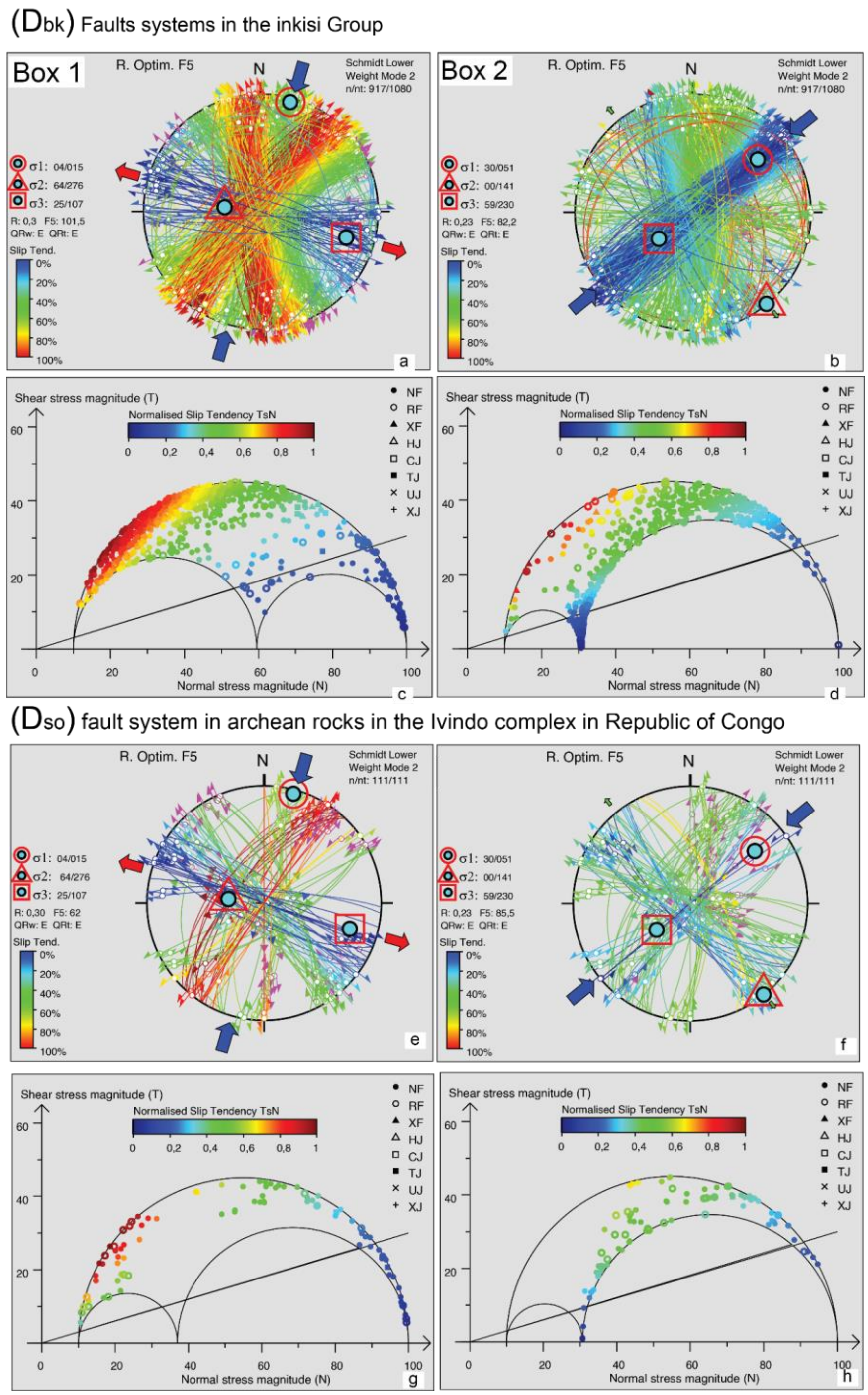

Figure 7: *The application of the stress inversion results for Box 1 (left column) and Box 2 (right column) on Dbk and Dso fault systems and the resulting Slip Tendency values associated with their Mohr-Coulomb stress states. The slip tendency estimate associated with each fault segment is presented as color-coded planes in both the stereoplots and their adjoining Mohr diagrams.*

Table 1: *Stress parameters associated with the focal mechanism solution of earthquakes in Box 1, Box 2, and Box 3 in Figure 2b. n: number of data used, nt: total data, Pl & Az: plunge & azimuth of principal compressive stress tensors, R': index regime; Reg: Regime, QRfm: Quality rank of focal mechanism.*

Stress parameters	*n*	*nt*	*σ1*		*σ2*		*σ3*		*Reg*	*QRfm*	*R'*		*Shmax*	*Shmin*
			Pl	*Az*	*Pl*	*Az*	*Pl*	*Az*			*Value*	*meaning*		
Box 1- West Central	8	18	4	15	64	276	25	107	SS	B	1.75	Transpressive	14	102
Box 2- Continental interior	8	10	30	51	0	141	60	232	TF	B	2.2	Transpressive	49	40
Box 3- Western Coastal Margin	8	12	3	184	73	83	17	275	SS	B	1.87	Transpressive	3	93

Table S4. Field measurements along the Dwc2 (Dk+Dso) fault system, West-Congo Belt, Republic of Congo and Democratic Republic of Congo.

Plane a recorded in Dip/Dip Direction convention.

DataID	Type of struct	Plane	Line	Sense	Confidence
Dwc2a1	1	81/360	11/272	NS	C
Dwc2a2	2	70/290	21/208	NS	P
Dwc2a3	2	90/070	30/160	ND	P
Dwc2a4	1	90/040	01/310	ID	P
Dwc2a5	4	90/080		TJ	P
Dwc2a6	4	70/095		TJ	P
Dwc2a7	1	90/009	01/279	NS	C
Dwc2a8	1	90/009	02/279	NS	C
Dwc2a9	3	90/009	00/279	NS	C
Dwc2a10	1	85/075	01/345	ID	P
Dwc2a11	1	80/010	01/280	NS	P
Dwc2a12	1	80/014	01/284	NS	P
Dwc2a13	4	90/155		TJ	P
Dwc2a14	4	90/155		TJ	P
Dwc2a15	1	80/214	01/124	NS	P
Dwc2a16	2	60/310	24/235	NS	P
Dwc2a17	2	75/068	36/147	ND	P
Dwc2a18	3	75/325	03/236	NS	P
Dwc2a19	1	65/210	04/122	ID	S
Dwc2a20	1	60/165	11/082	ID	S
Dwc2a21	1	75/004	19/279	NS	C
Dwc2a22	4	84/231		MJ	P
Dwc2a23	4	80/134		MJ	P
Dwc2a24	4	76/230		MJ	P
Dwc2a25	4	85/150		MJ	P
Dwc2a26	4	80/228		MJ	P
Dwc2a27	4	00/142		MJ	P
Dwc2a28	4	90/296		DJ	P
Dwc2a29	3	90/296	00/206	ID	P
Dwc2a30	3	85/225	13/136	NS	P
Dwc2a31	3	86/222	21/134	NS	P
Dwc2a32	4	84/224		SJ	P
Dwc2a33	4	85/318		DJ	P
Dwc2a34	4	89/324		DJ	P
Dwc2a35	4	79/130		DJ	P
Dwc2a36	4	90/299		UJ	P
Dwc2a37	4	90/300		UJ	P
Dwc2a38	3	90/322	00/232	ID	C
Dwc2a39	3	85/330	06/059	ND	C
Dwc2a40	3	90/322	00/232	ID	C
Dwc2a41	3	90/322	00/232	ID	C
Dwc2a42	3	90/010	00/100	IS	C
Dwc2a43	3	90/010	00/100	IS	C
Dwc2a44	3	90/008	00/098	IS	C
Dwc2a45	3	90/038	00/128	IS	C
Dwc2a46	3	75/214	10/127	NS	C
Dwc2a47	3	85/032	04/302	NS	C
Dwc2a48	3	86/122	03/212	ND	C
Dwc2a49	3	80/150	16/237	ND	C
Dwc2a50	3	86/122	05/212	ND	C
Dwc2a51	3	90/308	08/218	ID	C
Dwc2a52	3	86/122	11/211	ND	C
Dwc2a53	3	90/010	00/100	IS	C
Dwc2a54	3	90/015	00/105	IS	C
Dwc2a55	3	90/012	00/102	IS	C
Dwc2a56	3	90/017	00/107	IS	C
Dwc2a57	4	25/190		XJ	X
Dwc2a58	3	90/338	00/248	ID	C
Dwc2a59	3	90/338	00/248	ID	C
Dwc2a60	3	90/335	00/245	ID	C
Dwc2a61	3	90/335	00/245	ID	C
Dwc2a62	3	85/224	02/314	IS	C
Dwc2a63	3	90/232	07/322	IS	C
Dwc2a64	3	90/216	08/306	IS	C
Dwc2a65	3	75/042	22/318	NS	C
Dwc2a66	3	90/334	00/244	ID	C
Dwc2a67	4	85/078		MJ	C
Dwc2a68	3	82/068	01/158	IS	C
Dwc2a69	4	85/066		MJ	C
Dwc2a70	3	90/060	00/150	IS	C
Dwc2a71	4	24/160		IJ	C

Legend	Meaning
MJ	Mouvement plane with extension
NS	Sinistral plane with extension
IS	Sinistral plane with reverse component
ID	Dextral plane with reverse compnent
DJ	Dextral plane with extension
TJ	extension fracture
XX	Unknown sense of mouvement
P	Probable sens of mouvement
C	Certain sens of mouvement
S	Supposed sens of mouvement

Type of struct	Meaning
1	Fault with striae
2	Conjugate fault
3	Shear plane with extension fracture
4	Fracture with mouvement

Dwc2a72	3	85/078	15/349	NS	C
Dwc2a73	2	70/068	08/155	ND	P
Dwc2a74	2	85/122	21/210	IS	P
Dwc2a75	1	70/068	24/148	IS	C
Dwc2a76	4	85/122		DJ	P
Dwc2a77	1	39/212	36/187	ID	C
Dwc2a78	3	90/324	00/234	NS	C
Dwc2a79	3	80/120	11/032	NS	C
Dwc2a80	3	85/142	04/052	NS	C
Dwc2a81	4	20/240		IJ	P
Dwc2a82	4	85/058		DJ	P
Dwc2a83	3	85/068	03/338	NS	C
Dwc2a84	3	85/050	04/320	NS	P
Dwc2a85	4	80/242		SJ	P
Dwc2a86	3	85/068	08/157	ND	P
Dwc2a87	3	85/050	04/140	ND	P
Dwc2a88	3	80/242	12/330	ND	P
Dwc2a89	1	40/208	37/183	ID	C
Dwc2a90	4	90/130		SJ	P
Dwc2a91	3	65/022	14/105	ND	C
Dwc2a92	3	90/128	00/218	IS	C
Dwc2a93	1	90/080	01/350	ID	C
Dwc2a94	1	90/116	02/026	NS	C
Dwc2a95	1	85/120	09/031	NS	C
Dwc2a96	1	85/120	09/031	NS	C
Dwc2a97	1	89/232	01/142	NS	C
Dwc2a98	1	89/232	02/142	ID	C
Dwc2a99	4	90/120		SJ	C
Dwc2a100	3	75/050	11/323	NS	C
Dwc2a101	1	80/058	01/148	IS	C
Dwc2a102	3	80/058	06/329	NS	C
Dwc2a103	3	80/068	31/152	ND	C
Dwc2a104	3	89/132	00/222	IS	C
Dwc2a105	3	80/068	09/156	ND	C
Dwc2a106	3	80/032	08/303	NS	C
Dwc2a107	4	90/242		DJ	P
Dwc2a108	4	80/120		SJ	P
Dwc2a109	3	80/120	16/207	ND	C
Dwc2a110	3	80/115	13/203	ND	C
Dwc2a111	3	80/110	13/198	ND	C
Dwc2a112	3	80/118	14/206	ND	C
Dwc2a113	4	40/208		IJ	C
Dwc2a114	1	39/212	36/184	ID	P
Dwc2a115	1	25/206	23/183	ID	P
Dwc2a116	1	40/207	37/179	ID	P
Dwc2a117	1	35/204	34/186	ID	P
Dwc2a118	1	25/214	22/182	ID	P
Dwc2a119	1	29/200	28/182	ID	P
Dwc2a120	1	25/228	18/182	ID	P
Dwc2a121	1	30/208	28/186	ID	P
Dwc2a122	3	90/238	00/328	IS	C
Dwc2a123	3	90/237	00/327	IS	C
Dwc2a124	4	90/160		MJ	C
Dwc2a125	4	90/152		MJ	C
Dwc2a126	4	90/164		MJ	C
Dwc2a127	1	85/240	04/150	NS	C
Dwc2a128	1	75/232	05/143	NS	P
Dwc2a129	1	90/224	05/134	NS	P
Dwc2a130	1	85/250	16/338	IS	P
Dwc2a131	3	85/328	03/058	ND	C
Dwc2a132	1	85/142	20/054	ID	C
Dwc2a133	1	85/330	01/060	ND	C
Dwc2a134	3	90/206	00/116	NS	C
Dwc2a135	3	90/206	00/116	NS	C
Dwc2a136	4	90/320		DJ	S
Dwc2a137	4	90/318		DJ	S
Dwc2a138	4	85/230		MJ	P
Dwc2a139	4	85/232		MJ	P
Dwc2a140	4	85/234		MJ	P
Dwc2a141	1	85/232	06/321	IS	C
Dwc2a142	1	90/058	00/148	IS	C
Dwc2a143	4	86/150		MJ	P
Dwc2a144	3	86/064	04/334	NS	C
Dwc2a145	3	65/064	21/344	NS	C
Dwc2a146	3	75/068	12/341	NS	C
Dwc2a147	3	75/068	12/341	NS	C
Dwc2a148	3	68/062	05/334	NS	C
Dwc2a149	3	90/240	06/150	NS	C

Dwc2a150	3	88/232	08/142	NS	C
Dwc2a151	3	90/325	07/235	ID	P
Dwc2a152	4	80/232		MJ	C
Dwc2a153	4	85/134		MJ	C
Dwc2a154	3	85/238	16/149	NS	C
Dwc2a155	1	85/238	06/149	NS	C
Dwc2a156	1	82/229	05/318	IS	C
Dwc2a157	3	85/052	04/322	NS	C
Dwc2a158	3	80/058	06/329	NS	C
Dwc2a159	3	90/058	13/148	IS	C
Dwc2a160	4	90/060		SJ	C
Dwc2a161	4	85/068		SJ	C
Dwc2a162	4	89/248		SJ	C
Dwc2a163	4	85/330		MJ	C
Dwc2a164	4	90/154		MJ	C
Dwc2a165	4	90/060		SJ	C
Dwc2a166	1	89/052	06/142	IS	C
Dwc2a167	3	90/060	01/330	NS	C
Dwc2a168	3	82/232	06/143	NS	C
Dwc2a169	3	82/152	06/241	ND	C
Dwc2a170	3	83/150	06/239	ND	C
Dwc2a171	4	81/312		DJ	S
Dwc2a172	1	90/056	02/326	NS	P
Dwc2a173	4	89/322		DJ	P
Dwc2a174	3	85/150	02/060	ID	P
Dwc2a175	3	85/145	03/055	ID	P
Dwc2a176	1	85/150	06/239	ND	C
Dwc2a177	1	90/145	02/054	ID	C
Dwc2a178	4	89/332		DJ	P
Dwc2a179	1	86/232	11/142	ID	P
Dwc2a180	1	82/142	05/053	NS	P
Dwc2a181	1	85/230	01/140	ID	P
Dwc2a182	1	85/152	01/062	NS	P
Dwc2a183	3	85/230	14/141	NS	P
Dwc2a184	1	90/139	01/049	NS	P
Dwc2a185	1	85/220	01/130	ID	P
Dwc2a186	1	80/148	00/238	IS	P
Dwc2a187	3	90/250	00/160	NS	P
Dwc2a188	3	90/333	09/243	NS	P
Dwc2a189	3	90/333	13/243	NS	P
Dwc2a190	3	90/333	08/063	ND	P
Dwc2a191	3	84/333	25/060	ND	P
Dwc2a192	3	80/232	08/143	NS	C
Dwc2a193	3	90/144	00/234	ND	C
Dwc2a194	3	90/144	00/234	IS	C
Dwc2a195	4	90/062		SJ	P
Dwc2a196	3	90/124	13/214	IS	P
Dwc2a197	4	85/040		MJ	P
Dwc2a198	1	85/122	01/032	NS	P
Dwc2a199	1	85/122	01/033	NS	P
Dwc2a200	1	85/124	01/034	NS	P
Dwc2a201	3	65/122	51/068	NS	P
Dwc2a202	1	65/122	05/034	NS	S
Dwc2a203	1	65/124	04/036	NS	S
Dwc2a204	4	85/142		MJ	P
Dwc2a205	4	80/232		DJ	S
Dwc2a206	1	85/132	01/042	NS	P
Dwc2a207	4	70/054		DJ	S
Dwc2a208	4	85/142		SJ	P
Dwc2a209	4	90/236		DJ	P
Dwc2a210	3	75/130	25/047	NS	P
Dwc2a211	3	65/120	46/059	NS	P
Dwc2a212	3	85/150	04/060	NS	P
Dwc2a213	1	90/226	01/136	ID	P
Dwc2a214	1	80/222	05/133	ID	P
Dwc2a215	1	85/230	05/140	ID	P
Dwc2a216	3	89/058	07/328	NS	P
Dwc2a217	3	89/058	07/148	ND	P
Dwc2a218	3	80/152	03/063	NS	P
Dwc2a219	1	80/152	01/062	NS	C
Dwc2a220	4	80/052		MJ	C
Dwc2a221	4	85/242		MJ	C
Dwc2a222	4	85/320		MJ	C
Dwc2a223	4	80/330		MJ	C
Dwc2a224	4	90/229		MJ	C
Dwc2a225	4	85/230		DJ	C
Dwc2a226	1	85/230	01/140	ID	C
Dwc2a227	4	85/320		SJ	P

Dwc2a228	4	85/064		MJ	P
Dwc2a229	1	85/142	11/053	NS	P
Dwc2a230	1	85/142	85/142	NX	P
Dwc2a231	4	85/050		MJ	P
Dwc2a232	3	80/050	04/321	ID	C
Dwc2a233	3	80/050	08/139	ND	C
Dwc2a234	3	80/050	08/139	ND	C
Dwc2a235	3	90/230	00/320	ND	C
Dwc2a236	3	90/230	12/320	ND	C
Dwc2a237	4	80/242		MJ	P
Dwc2a238	4	85/154		MJ	P
Dwc2a239	3	80/068	04/339	ID	P
Dwc2a240	3	80/250	15/337	ND	P
Dwc2a241	4	90/312		MJ	P
Dwc2a242	4	90/042		MJ	P
Dwc2a243	4	85/039		DJ	P
Dwc2a244	1	85/292	00/202	ID	P
Dwc2a245	1	85/294	00/024	ND	P
Dwc2a246	4	80/122		MJ	C
Dwc2a247	4	80/312		MJ	C
Dwc2a248	4	90/290		MJ	C
Dwc2a249	4	75/292		MJ	C
Dwc2a250	4	82/209		MJ	C
Dwc2a251	4	85/022		MJ	C
Dwc2a252	4	65/050		MJ	C
Dwc2a253	3	90/300	23/210	NS	S
Dwc2a254	1	90/300	00/210	ID	P
Dwc2a255	4	85/108		DJ	P
Dwc2a256	1	85/252	05/162	NS	P
Dwc2a257	4	90/247		MJ	C
Dwc2a258	4	90/120		MJ	C
Dwc2a259	4	90/124		MJ	C
Dwc2a260	1	85/295	05/205	NS	P
Dwc2a261	1	90/124	05/214	IS	P
Dwc2a262	1	80/132	05/042	ID	P
Dwc2a263	3	90/110	00/020	NS	P
Dwc2a264	1	90/110	07/020	NS	P
Dwc2a265	4	89/284		MJ	P
Dwc2a266	1	85/216	05/126	NS	P
Dwc2a267	4	89/119		MJ	P
Dwc2a268	4	90/292		MJ	P
Dwc2a269	4	80/292		DJ	P
Dwc2a270	4	80/292		SJ	P
Dwc2a271	4	85/294		MJ	P
Dwc2a272	4	84/294		MJ	P
Dwc2a273	4	75/029		MJ	P
Dwc2a274	1	89/112	05/022	NS	P
Dwc2a275	1	85/182	00/272	ND	P
Dwc2a276	2	65/004	48/063	ND	P
Dwc2a277	2	80/207	56/132	NS	P
Dwc2a278	4	80/220		MJ	C
Dwc2a279	4	80/250		MJ	C
Dwc2a280	4	78/196		MJ	C
Dwc2a281	4	90/170		MJ	C
Dwc2a282	1	80/110	05/020	ID	P
Dwc2a283	1	89/308	01/218	ID	P
Dwc2a284	1	85/050	01/320	NS	P
Dwc2a285	1	85/312	02/222	ID	P
Dwc2a286	1	89/288	02/198	ID	P
Dwc2a287	4	85/030		MJ	C
Dwc2a288	4	85/052		SJ	S
Dwc2a289	4	80/050		SJ	S
Dwc2a290	3	89/090	01/180	ND	C
Dwc2a291	3	90/270	13/360	IS	C
Dwc2a292	3	90/270	13/360	IS	C
Dwc2a293	3	85/132	04/042	NS	C
Dwc2a294	3	89/328	01/238	NS	C
Dwc2a295	4	89/328		DJ	C
Dwc2a296	3	85/126	10/037	NS	C
Dwc2a297	3	85/126	05/036	NS	C
Dwc2a298	3	85/126	05/216	ND	C
Dwc2a299	4	90/042		DJ	C
Dwc2a300	4	90/150		MJ	C
Dwc2a301	4	90/052		MJ	C
Dwc2a302	4	90/088		MJ	C
Dwc2a303	4	90/169		DJ	C
Dwc2a304	4	90/162		DJ	C
Dwc2a305	1	85/130	05/040	NS	P

Dwc2a306	1	75/068	05/157	ND	P
Dwc2a307	1	90/228	03/138	ID	P
Dwc2a308	1	89/168	05/078	NS	P
Dwc2a309	4	85/308		DJ	P
Dwc2a310	4	75/116		DJ	P
Dwc2a311	4	69/121		DJ	P
Dwc2a312	1	86/110	06/020	ID	P
Dwc2a313	1	85/286	06/015	ND	P
Dwc2a314	1	90/262	30/172	ID	P
Dwc2a315	1	90/262	00/172	ID	P
Dwc2a316	4	90/264		MJ	P
Dwc2a317	1	84/290	01/200	ID	P
Dwc2a318	1	89/059	00/149	IS	P
Dwc2a319	1	85/240	02/151	ID	P
Dwc2a320	3	85/240	09/329	ND	P
Dwc2a321	1	85/240	06/329	ND	C
Dwc2a322	1	89/084	05/354	ID	C
Dwc2a323	4	89/268		MJ	C
Dwc2a324	4	89/101		MJ	C
Dwc2a325	4	90/304		MJ	C
Dwc2a326	4	89/084		MJ	C
Dwc2a327	1	30/068	29/080	IS	S
Dwc2a328	4	90/222		MJ	C
Dwc2a329	4	90/300		MJ	C
Dwc2a330	4	35/210		IJ	P
Dwc2a331	1	75/124	14/038	ID	C
Dwc2a332	1	76/125	10/038	ID	C
Dwc2a333	1	76/130	09/042	ID	C
Dwc2a334	1	75/125	04/036	ID	C
Dwc2a335	4	90/052		MJ	C
Dwc2a336	4	75/150		MJ	C
Dwc2a337	4	85/050		SJ	S
Dwc2a338	1	90/050	02/320	NS	S
Dwc2a339	4	90/140		MJ	C
Dwc2a340	1	85/130	00/040	ID	C
Dwc2a341	3	85/140	04/230	ND	C
Dwc2a342	3	90/140	00/230	ND	C
Dwc2a343	3	85/058	03/328	NS	C
Dwc2a344	3	90/050	00/140	IS	C
Dwc2a345	1	90/062	02/332	NS	C
Dwc2a346	1	90/064	02/334	NS	C
Dwc2a347	4	90/132		DJ	P
Dwc2a348	4	85/132		DJ	P
Dwc2a349	4	90/120		DJ	P
Dwc2a350	1	90/128	05/218	ND	C
Dwc2a351	1	90/132	02/042	ID	C
Dwc2a352	1	90/128	02/038	ID	C
Dwc2a353	1	90/132	06/222	ND	C
Dwc2a354	4	80/138		DJ	P
Dwc2a355	4	70/060		SJ	P
Dwc2a356	4	85/058		SJ	P
Dwc2a357	4	79/050		SJ	P
Dwc2a358	4	35/050		IJ	P
Dwc2a359	4	72/120		DJ	P
Dwc2a360	4	85/138		DJ	P
Dwc2a361	4	90/115		DJ	P
Dwc2a362	3	89/125	07/215	ND	P
Dwc2a363	1	85/120	02/210	ND	C
Dwc2a364	1	85/114	02/204	ND	C
Dwc2a365	4	90/352		DJ	C
Dwc2a366	4	65/348		DJ	P
Dwc2a367	4	85/350		DJ	P
Dwc2a368	1	75/140	05/229	ND	C
Dwc2a369	1	90/300	05/210	ID	C
Dwc2a370	1	90/304	05/214	ID	C
Dwc2a371	4	75/238		SJ	S
Dwc2a372	4	90/240		SJ	S
Dwc2a373	1	90/312	10/222	ID	C
Dwc2a374	1	90/314	10/224	ID	C
Dwc2a375	4	85/244		SJ	S
Dwc2a376	1	90/132	05/222	ND	C
Dwc2a377	4	85/332		DJ	C
Dwc2a378	4	85/330		DJ	C
Dwc2a379	4	90/310		DJ	C
Dwc2a380	1	85/140	05/230	ND	C
Dwc2a381	1	80/134	05/224	ND	C
Dwc2a382	1	85/134	08/224	ND	C
Dwc2a383	1	85/140	05/050	ID	C

Dwc2a384	1	80/134	06/045	ID	C
Dwc2a385	4	30/214		IJ	C
Dwc2a386	4	85/138		MJ	P
Dwc2a387	4	90/082		MJ	P
Dwc2a388	4	89/188		SJ	S
Dwc2a389	1	78/182	00/272	IS	P
Dwc2a390	1	85/300	15/211	ID	P
Dwc2a391	4	79/079		MJ	P
Dwc2a392	1	85/272	18/184	ID	P
Dwc2a393	4	80/009		SJ	P
Dwc2a394	1	73/089	02/178	ND	P
Dwc2a395	4	80/250		MJ	P
Dwc2a396	1	85/262	02/172	ID	P
Dwc2a397	4	80/180		MJ	P
Dwc2a398	1	80/240	00/150	ID	P
Dwc2a399	4	79/110		MJ	P
Dwc2a400	4	80/258		MJ	P
Dwc2a401	1	80/348	11/076	IS	P
Dwc2a402	4	85/240		DJ	P
Dwc2a403	4	82/270		MJ	P
Dwc2a404	4	85/075		DJ	S
Dwc2a405	4	89/300		DJ	P
Dwc2a406	4	82/162		MJ	P
Dwc2a407	4	75/118		MJ	P
Dwc2a408	1	90/270	12/180	ID	P
Dwc2a409	1	85/258	02/168	ID	P
Dwc2a410	1	78/178	02/088	NS	P
Dwc2a411	1	75/342	09/070	IS	P
Dwc2a412	4	85/262		MJ	P
Dwc2a413	4	80/082		MJ	P
Dwc2a414	4	79/081		MJ	P
Dwc2a415	1	85/262	12/173	ID	P
Dwc2a416	4	85/148		MJ	S
Dwc2a417	1	75/172	01/082	NS	P
Dwc2a418	4	80/062		DJ	S
Dwc2a419	4	79/080		MJ	P
Dwc2a420	4	79/082		MJ	P
Dwc2a421	4	89/128		BJ	C
Dwc2a422	4	85/290		BJ	C
Dwc2a423	4	83/296		BJ	C
Dwc2a424	4	90/290		BJ	C
Dwc2a425	4	89/034		BJ	C
Dwc2a426	4	75/058		MJ	C
Dwc2a427	4	72/334		MJ	C
Dwc2a428	4	80/240		MJ	C
Dwc2a429	4	76/338		MJ	C
Dwc2a430	4	75/077		MJ	C
Dwc2a431	4	80/242		MJ	C
Dwc2a432	4	82/242		MJ	C
Dwc2a433	4	75/340		MJ	C
Dwc2a434	4	70/342		MJ	C
Dwc2a435	4	85/000		MJ	C
Dwc2a436	4	90/358		MJ	C
Dwc2a437	4	85/276		MJ	C
Dwc2a438	4	80/170		MJ	C
Dwc2a439	4	89/070		MJ	C
Dwc2a440	3	89/332	04/062	ND	C
Dwc2a441	3	90/062	18/332	NS	C
Dwc2a442	3	90/252	15/342	IS	C
Dwc2a443	4	90/240		SJ	P
Dwc2a444	4	89/002		DJ	P
Dwc2a445	4	89/000		DJ	P
Dwc2a446	4	84/000		DJ	P
Dwc2a447	4	90/174		DJ	P
Dwc2a448	4	80/340		DJ	P
Dwc2a449	4	90/252		SJ	P
Dwc2a450	4	90/252		SJ	P
Dwc2a451	4	90/154		DJ	P
Dwc2a452	3	90/252	00/342	IS	P
Dwc2a453	4	75/115		MJ	C
Dwc2a454	4	64/144		MJ	C
Dwc2a455	3	85/252	04/342	IS	C
Dwc2a456	4	80/140		DJ	S
Dwc2a457	4	87/144		DJ	S
Dwc2a458	3	82/055	19/328	NS	P
Dwc2a459	4	90/229		SJ	C
Dwc2a460	4	80/212		SJ	C
Dwc2a461	3	90/046	12/316	NS	C

Dwc2a462	3	90/046	18/136	IS	C
Dwc2a463	4	82/062		SJ	P
Dwc2a464	4	85/152		DJ	P
Dwc2a465	4	90/150		DJ	P
Dwc2a466	4	90/230		SJ	P
Dwc2a467	3	90/045	00/315	NS	P
Dwc2a468	3	90/229	00/139	NS	C
Dwc2a469	3	90/054	00/144	IS	C
Dwc2a470	4	90/052		SJ	C
Dwc2a471	4	90/229		SJ	C
Dwc2a472	3	85/060	09/149	IS	C
Dwc2a473	4	90/038		SJ	P
Dwc2a474	3	90/048	00/138	IS	P
Dwc2a475	3	90/232	00/142	NS	P
Dwc2a476	4	90/058		SJ	P
Dwc2a477	4	86/052		SJ	P
Dwc2a478	4	86/060		SJ	P
Dwc2a479	4	85/248		SJ	P
Dwc2a480	4	80/232		SJ	P
Dwc2a481	4	90/230		SJ	P
Dwc2a482	4	90/058		SJ	P
Dwc2a483	4	90/338		DJ	P
Dwc2a484	3	90/338	00/248	ID	P
Dwc2a485	4	90/068		SJ	P
Dwc2a486	4	90/068		SJ	P
Dwc2a487	4	90/320		DJ	P
Dwc2a488	4	85/050		SJ	P
Dwc2a489	4	90/150		DJ	P
Dwc2a490	4	85/053		SJ	P
Dwc2a491	4	90/060		SJ	P
Dwc2a492	4	90/060		SJ	P
Dwc2a493	4	90/058		SJ	P
Dwc2a494	4	90/048		SJ	P
Dwc2a495	4	90/238		SJ	P
Dwc2a496	4	90/060		SJ	P
Dwc2a497	4	90/312		DJ	P
Dwc2a498	4	90/062		SJ	P
Dwc2a499	4	90/050		SJ	P
Dwc2a500	4	90/034		SJ	P
Dwc2a501	4	90/054		SJ	P
Dwc2a502	3	85/238	03/148	NS	P
Dwc2a503	4	85/146		MJ	C
Dwc2a504	1	90/040	00/130	IS	C
Dwc2a505	4	90/070		SJ	C
Dwc2a506	4	90/312		MJ	P
Dwc2a507	4	90/062		MJ	P
Dwc2a508	4	85/146		MJ	P
Dwc2a509	4	85/146		MJ	P
Dwc2a510	3	80/232	07/143	NS	C
Dwc2a511	3	90/229	00/139	NS	C
Dwc2a512	4	90/148		MJ	C
Dwc2a513	4	80/050		SJ	P
Dwc2a514	4	89/312		MJ	P
Dwc2a515	4	90/062		SJ	C
Dwc2a516	3	90/232	00/322	IS	C
Dwc2a517	3	90/232	00/322	IS	C
Dwc2a518	1	86/062	00/152	IS	C
Dwc2a519	3	87/061	02/331	NS	C
Dwc2a520	3	86/061	03/331	NS	C
Dwc2a521	3	90/237	00/147	NS	C
Dwc2a522	4	90/238		SJ	C
Dwc2a523	3	90/235	00/145	NS	C
Dwc2a524	2	51/252	51/253	ND	C
Dwc2a525	2	56/073	56/072	NS	C
Dwc2a526	4	90/248		SJ	C
Dwc2a527	4	85/230		MJ	C
Dwc2a528	3	82/050	06/321	NS	C
Dwc2a529	4	80/058		SJ	C
Dwc2a530	4	90/053		SJ	C
Dwc2a531	4	82/242		SJ	C
Dwc2a532	4	90/340		MJ	C
Dwc2a533	4	90/148		DJ	C
Dwc2a534	4	90/088		DJ	C
Dwc2a535	4	89/332		MJ	C
Dwc2a536	4	89/148		MJ	C
Dwc2a537	4	82/072		SJ	C
Dwc2a538	4	80/060		SJ	C
Dwc2a539	4	80/055		SJ	C

Dwc2a540	4	76/094		SJ	C
Dwc2a541	4	75/102		SJ	C
Dwc2a542	4	80/152		MJ	C
Dwc2a543	4	79/148		MJ	C
Dwc2a544	4	85/155		MJ	C
Dwc2a545	4	89/332		MJ	C
Dwc2a546	4	85/154		MJ	C
Dwc2a547	3	82/058	08/147	IS	C
Dwc2a548	2	75/042	74/058	ND	C
Dwc2a549	2	66/225	66/214	NS	C
Dwc2a550	4	89/272		MJ	P
Dwc2a551	3	90/242	00/152	NS	C
Dwc2a552	2	75/050	66/103	ND	C
Dwc2a553	2	75/240	66/187	NS	C
Dwc2a554	4	86/136		DJ	C
Dwc2a555	4	90/150		DJ	P
Dwc2a556	4	85/158		DJ	P
Dwc2a557	4	80/152		DJ	P
Dwc2a558	4	80/142		DJ	P
Dwc2a559	4	85/048		MJ	C
Dwc2a560	4	80/060		MJ	C
Dwc2a561	3	85/058	03/328	NS	C
Dwc2a562	3	85/058	03/328	NS	C
Dwc2a563	4	86/062		SJ	C
Dwc2a564	4	90/128		MJ	C
Dwc2a565	4	85/140		MJ	C
Dwc2a566	4	90/040		SJ	C
Dwc2a567	4	79/054		MJ	C
Dwc2a568	4	89/232		MJ	C
Dwc2a569	4	80/130		MJ	C
Dwc2a570	4	86/152		MJ	C
Dwc2a571	4	86/150		MJ	C
Dwc2a572	4	86/160		MJ	C
Dwc2a573	4	84/160		MJ	C
Dwc2a574	4	84/140		MJ	C
Dwc2a575	3	80/150	04/239	ND	C
Dwc2a576	3	80/150	02/060	ID	C
Dwc2a577	4	82/241		MJ	C
Dwc2a578	3	86/062	03/332	NS	C
Dwc2a579	4	72/258		MJ	C
Dwc2a580	3	85/168	10/257	ND	C
Dwc2a581	3	80/000	08/089	ND	C
Dwc2a582	3	90/350	00/080	ND	C
Dwc2a583	3	90/350	00/080	ND	C
Dwc2a584	4	90/270		MJ	P
Dwc2a585	4	90/130		DJ	P
Dwc2a586	4	90/104		DJ	P
Dwc2a587	1	85/172	00/262	ND	C
Dwc2a588	1	90/006	00/096	ND	C
Dwc2a589	3	90/000	00/270	ID	C
Dwc2a590	3	90/000	00/270	ID	C
Dwc2a591	3	90/183	00/273	ND	C
Dwc2a592	4	90/134		DJ	C
Dwc2a593	1	90/168	00/258	ND	C
Dwc2a594	1	90/146	00/236	ND	C
Dwc2a595	1	90/158	00/248	ND	C
Dwc2a596	1	90/140	00/230	ND	C
Dwc2a597	3	90/270	06/180	ID	C
Dwc2a598	4	80/086		DJ	S
Dwc2a599	4	75/138		DJ	S
Dwc2a600	3	80/142	03/232	IS	P
Dwc2a601	4	80/348		SJ	P
Dwc2a602	3	80/312	39/230	NS	P
Dwc2a603	3	90/151	00/241	IS	P
Dwc2a604	3	90/110	00/020	ID	P
Dwc2a605	4	90/098		DJ	P
Dwc2a606	4	90/168		MJ	P
Dwc2a607	4	90/058		MJ	P
Dwc2a608	4	90/108		DJ	P
Dwc2a609	4	90/114		MJ	P
Dwc2a610	4	90/054		MJ	P
Dwc2a611	4	90/158		MJ	P
Dwc2a612	4	90/138		MJ	P
Dwc2a613	3	90/152	00/062	ID	C
Dwc2a614	4	85/068		MJ	P
Dwc2a615	4	80/320		MJ	P
Dwc2a616	4	80/240		MJ	P
Dwc2a617	3	90/142	00/052	ID	C

Dwc2a618	3	90/052	00/142	IS	C
Dwc2a619	4	90/058		SJ	P
Dwc2a620	4	90/148		DJ	P
Dwc2a621	4	90/142		DJ	P
Dwc2a622	3	90/142	06/052	ID	P
Dwc2a623	4	90/138		MJ	P
Dwc2a624	4	90/060		MJ	P
Dwc2a625	3	90/072	00/162	IS	P
Dwc2a626	3	90/070	00/160	IS	P
Dwc2a627	3	90/080	00/170	IS	P
Dwc2a628	3	90/080	00/170	IS	P
Dwc2a629	4	85/060		DJ	P
Dwc2a630	4	70/060		DJ	P
Dwc2a631	3	90/062	00/332	ID	C
Dwc2a632	3	90/148	00/238	ND	C
Dwc2a633	3	90/051	00/141	IS	C
Dwc2a634	3	90/051	00/141	IS	C
Dwc2a635	4	90/150		DJ	C
Dwc2a636	4	90/158		DJ	C
Dwc2a637	3	90/158	00/248	ND	C
Dwc2a638	3	90/158	00/248	ND	C
Dwc2a639	3	90/130	00/220	ND	C
Dwc2a640	3	90/136	00/226	ND	C
Dwc2a641	3	90/139	00/229	ND	C
Dwc2a642	3	90/139	00/229	ND	C
Dwc2a643	1	90/139	01/229	ND	C
Dwc2a644	3	90/059	00/149	IS	C
Dwc2a645	3	90/059	00/149	IS	C
Dwc2a646	3	90/064	00/154	IS	C
Dwc2a647	4	90/138		MJ	P
Dwc2a648	4	90/068		MJ	P
Dwc2a649	4	90/062		MJ	P
Dwc2a650	4	90/050		MJ	P
Dwc2a651	4	90/058		MJ	P
Dwc2a652	3	85/058	09/329	NS	C
Dwc2a653	4	90/238		MJ	P
Dwc2a654	4	90/070		MJ	P
Dwc2a655	3	90/068	00/338	ID	C
Dwc2a656	4	82/062		MJ	P
Dwc2a657	4	90/137		MJ	P
Dwc2a658	3	90/062	00/332	ID	C
Dwc2a659	3	90/062	00/332	ID	C
Dwc2a660	3	90/062	00/152	IS	C
Dwc2a661	3	90/068	00/158	IS	C
Dwc2a662	3	90/058	00/328	ID	C
Dwc2a663	3	90/049	00/319	ID	C
Dwc2a664	3	90/049	00/139	IS	C
Dwc2a665	3	90/060	00/150	IS	C
Dwc2a666	3	90/060	00/150	IS	C
Dwc2a667	1	90/060	01/150	IS	C
Dwc2a668	3	90/139	00/229	ND	C
Dwc2a669	3	90/130	00/220	ND	C
Dwc2a670	3	90/068	00/158	IS	C
Dwc2a671	4	90/060		MJ	P
Dwc2a672	4	90/058		MJ	P
Dwc2a673	4	90/142		MJ	P
Dwc2a674	3	90/130	00/220	ND	C
Dwc2a675	3	90/068	00/158	IS	C
Dwc2a676	3	90/069	00/159	IS	C
Dwc2a677	4	90/158		MJ	C
Dwc2a678	3	90/078	00/168	IS	C
Dwc2a679	4	90/144		MJ	C
Dwc2a680	4	90/162		MJ	C
Dwc2a681	3	90/070	00/340	ID	C
Dwc2a682	3	90/074	00/164	IS	C
Dwc2a683	3	90/074	00/164	IS	C
Dwc2a684	3	90/072	00/162	IS	C
Dwc2a685	3	90/150	00/240	ND	C
Dwc2a686	3	90/078	00/168	IS	C
Dwc2a687	3	90/068	00/158	IS	C
Dwc2a688	3	90/150	00/240	ND	C
Dwc2a689	4	90/050		MJ	C
Dwc2a690	3	90/061	00/331	ID	C
Dwc2a691	3	90/066	00/156	IS	C
Dwc2a692	4	90/068		SJ	P
Dwc2a693	4	90/056		SJ	P
Dwc2a694	3	90/050	00/320	ID	C
Dwc2a695	4	90/042		SJ	C

Dwc2a696	3	90/062	00/152	IS	C
Dwc2a697	1	90/062	10/152	IS	C
Dwc2a698	3	90/040	00/310	ID	C
Dwc2a699	1	90/064	10/154	ND	P
Dwc2a700	3	90/062	00/332	ID	P
Dwc2a701	3	90/062	00/332	ID	P
Dwc2a702	4	90/062		MJ	P
Dwc2a703	3	90/058	00/328	ID	C
Dwc2a704	3	90/049	00/319	ID	C
Dwc2a705	3	90/158	00/248	ND	C
Dwc2a706	3	90/162	00/252	IS	C
Dwc2a707	3	90/161	00/251	ND	C
Dwc2a708	3	90/158	00/248	IS	C
Dwc2a709	3	90/161	00/251	IS	C
Dwc2a710	3	90/158	00/248	ND	C
Dwc2a711	3	90/158	00/248	ND	C
Dwc2a712	3	90/158	00/248	IS	C
Dwc2a713	1	90/148	01/238	ND	C
Dwc2a714	3	90/068	00/158	IS	C
Dwc2a715	4	90/352		MJ	C
Dwc2a716	4	90/060		MJ	C
Dwc2a717	4	85/330		MJ	C
Dwc2a718	4	90/068		MJ	C
Dwc2a719	4	90/160		MJ	C
Dwc2a720	3	90/080	00/170	IS	C
Dwc2a721	3	90/060	00/150	IS	C
Dwc2a722	4	90/050		MJ	C
Dwc2a723	4	90/072		MJ	C
Dwc2a724	3	90/054	00/144	IS	C
Dwc2a725	1	90/162	00/252	ND	P
Dwc2a726	1	90/114	00/204	IS	P
Dwc2a727	1	90/125	00/215	IS	P
Dwc2a728	1	90/125	00/215	IS	P
Dwc2a729	1	90/180	00/090	ID	P
Dwc2a730	1	90/170	10/080	ID	P
Dwc2a731	1	90/180	00/090	ID	P
Dwc2a732	1	80/180	00/090	ID	P
Dwc2a733	1	70/178	05/090	ID	P
Dwc2a734	1	89/177	05/087	ID	P
Dwc2a735	2	88/320	01/050	IS	P
Dwc2a736	2	88/261	01/171	ID	P
Dwc2a737	2	89/321	05/051	IS	P
Dwc2a738	2	85/255	01/345	ND	P
Dwc2a739	2	89/327	01/237	NS	P
Dwc2a740	2	89/076	01/166	ND	P
Dwc2a741	2	89/330	03/240	NS	P
Dwc2a742	2	87/070	02/160	ND	P
Dwc2a743	2	85/328	04/058	IS	P
Dwc2a744	2	85/248	04/158	ID	P
Dwc2a745	2	89/165	02/255	IS	P
Dwc2a746	2	88/090	00/000	ID	P
Dwc2a747	2	89/165	05/255	IS	P
Dwc2a748	2	85/092	00/182	ND	P
Dwc2a749	2	88/255	05/345	ND	S
Dwc2a750	2	85/155	03/065	NS	S
Dwc2a751	2	85/259	10/170	ID	S
Dwc2a752	2	79/336	02/066	IS	S
Dwc2a753	2	76/248	10/160	ID	S
Dwc2a754	2	78/330	12/057	IS	S
Dwc2a755	2	85/082	12/171	ND	S
Dwc2a756	2	80/334	08/245	NS	S
Dwc2a757	2	85/262	06/351	ND	S
Dwc2a758	2	85/158	06/069	NS	S
Dwc2a759	2	89/093	35/004	ID	P
Dwc2a760	2	68/127	26/048	NS	P
Dwc2a761	2	85/080	09/351	ID	P
Dwc2a762	2	80/123	03/034	NS	P
Dwc2a763	2	89/120	07/210	ND	P
Dwc2a764	2	85/349	06/259	NS	P
Dwc2a765	2	78/147	44/069	NS	P
Dwc2a766	2	86/300	09/211	ID	P
Dwc2a767	2	80/358	02/268	NS	P
Dwc2a768	2	85/307	09/036	IS	P
Dwc2a769	2	80/253	01/343	ND	P
Dwc2a770	4	83/284		MJ	P
Dwc2a771	4	86/051		MJ	P
Dwc2a772	4	88/122		MJ	P
Dwc2a773	4	80/347		MJ	P

Dwc2a774	4	88/349		MJ	P
Dwc2a775	4	78/162		MJ	P
Dwc2a776	4	82/342		MJ	P
Dwc2a777	4	45/114		MJ	P
Dwc2a778	4	35/120		MJ	P
Dwc2a779	4	59/112		MJ	P
Dwc2a780	4	55/122		MJ	P
Dwc2a781	4	58/138		MJ	P
Dwc2a782	4	65/122		MJ	P
Dwc2a783	4	66/256		MJ	P
Dwc2a784	4	64/240		MJ	P
Dwc2a785	4	60/044		MJ	P
Dwc2a786	4	85/336		MJ	P
Dwc2a787	4	89/235		MJ	P
Dwc2a788	4	86/238		MJ	P
Dwc2a789	4	88/348		MJ	C
Dwc2a790	4	68/145		MJ	P
Dwc2a791	4	80/235		MJ	P
Dwc2a792	2	85/175	03/085	ID	P
Dwc2a793	2	85/241	03/331	IS	P
Dwc2a794	2	82/190	02/280	ND	P
Dwc2a795	2	86/239	07/328	IS	P
Dwc2a796	2	83/340	03/070	ND	P
Dwc2a797	2	88/240	07/150	NS	P
Dwc2a798	4	88/166		MJ	P
Dwc2a799	4	88/058		MJ	P
Dwc2a800	4	89/345		MJ	P
Dwc2a801	4	89/351		MJ	P
Dwc2a802	4	85/238		MJ	P
Dwc2a803	4	89/345		MJ	P
Dwc2a804	1	30/054	11/343	ID	C
Dwc2a805	1	31/043	17/344	ID	C
Dwc2a806	1	43/002	38/330	ID	C
Dwc2a807	1	51/359	38/308	ID	C
Dwc2a808	1	50/029	32/330	ID	C
Dwc2a809	1	30/170	29/160	ID	C
Dwc2a810	1	50/177	44/142	ID	P
Dwc2a811	1	18/141	18/147	IS	P
Dwc2a812	1	33/123	31/145	IS	S
Dwc2a813	1	52/012	42/327	ID	S
Dwc2a814	1	40/355	36/326	ID	S
Dwc2a815	4	42/297		IJ	S
Dwc2a816	4	88/237		MJ	P
Dwc2a817	1	22/118	17/160	IS	C
Dwc2a818	1	21/149	21/155	IS	C
Dwc2a819	1	22/159	21/142	ID	C
Dwc2a820	1	45/260	11/181	ID	C
Dwc2a821	1	55/276	05/190	ID	C
Dwc2a822	1	57/283	03/011	ND	C
Dwc2a823	1	55/266	10/183	ID	P
Dwc2a824	1	60/282	02/193	ID	C
Dwc2a825	1	70/272	03/001	ND	C
Dwc2a826	1	55/294	01/024	ND	C
Dwc2a827	4	41/165		MJ	C
Dwc2a828	4	25/149		MJ	C
Dwc2a829	2	78/338	03/067	IS	P
Dwc2a830	2	85/257	11/168	ID	P
Dwc2a831	2	78/338	03/067	IS	P
Dwc2a832	2	85/257	11/168	ID	P
Dwc2a833	1	82/282	07/011	IS	C
Dwc2a834	1	78/293	14/020	IS	C
Dwc2a835	1	83/124	08/035	NS	C
Dwc2a836	1	75/293	11/020	IS	C
Dwc2a837	1	80/282	09/010	IS	C
Dwc2a838	4	80/245		TJ	C
Dwc2a839	4	80/256		TJ	C
Dwc2a840	4	80/314		SJ	P
Dwc2a841	4	90/120		SJ	P
Dwc2a842	4	80/130		SJ	P
Dwc2a843	4	80/048		DJ	P
Dwc2a844	4	85/050		DJ	P
Dwc2a845	4	72/304		SJ	P
Dwc2a846	4	72/324		MJ	C
Dwc2a847	2	58/292	49/248	NS	C
Dwc2a848	2	59/082	50/127	ND	C
Dwc2a849	2	72/304	18/220	NS	C
Dwc2a850	2	80/060	23/146	ND	C
Dwc2a851	2	72/304	17/220	NS	C

Dwc2a852	2	80/058	23/144	ND	C
Dwc2a853	2	73/310	15/225	NS	C
Dwc2a854	2	80/058	20/144	ND	C
Dwc2a855	3	82/310	00/220	NS	C
Dwc2a856	3	82/320	05/231	NS	C
Dwc2a857	3	82/310	13/222	NS	C
Dwc2a858	4	80/058		DJ	P
Dwc2a859	4	85/055		DJ	P